SLAC-PUB-2408
October 1979
(E)

DIMUON PRODUCTION IN 15.5 GeV/c πp INTERACTIONS AND THE OBSERVATION OF A LOW-MASS CONTINUUM*

R. Cassell,† B. Haber, E. Kogan,†† W.C. Barber, K. Bunnell, M. Duong-van,‡ R. Mozley, A. Odian, R. Panvini, S. Poucher, T. Schalk, S. Stone, F. Villa, L. Wang‡‡

Stanford Linear Accelerator Center*
Stanford University, Stanford, California 94305

Vanderbilt University,** Nashville, Tennessee 37203

University of California-Santa Cruz*
Santa Cruz, California 95064

and

Massachusetts Institute of Technology
Cambridge, Massachusetts 02139

Submitted to Phys. Rev.

---

*Work supported in part by the Department of Energy under Contract No. DE-AC03-76SF00515 (SLAC) and under Contract No. EY-76-S-03-0034 (UC-SC).

**Work supported by the National Science Foundation and Grants by the Vanderbilt University Research Council.

†Now at University of Illinois, Resident at SLAC.

††Now at Weizmann Institute of Science, Rehovot, Israel.

‡Now at Los Alamos Scientific Laboratory, Los Alamos, New Mexico.

‡‡Now at C. M. Technologies, Palo Alto, California.

ABSTRACT

We report on a streamer chamber experiment which examines the entire final state of events in which muon pairs were produced in 15.5 GeV/c $\pi^{\pm}p$ interactions.

A portion of this data was presented earlier.[1] Here we report on the final data sample of 890 events obtained from a total of 2.5×10^8 interactions (a sensitivity of 8.65 events/nbarn × trigger efficiency).

The experiment was sensitive primarily to the low-mass region and the good mass resolution made it possible to identify the contributions from the ρ and ω decays and the η and ω Dalitz decays. An excess of events is observed in the dimuon mass region $\sim$ 400 - 600 MeV which is not accounted for by the above-mentioned decays.

The final states were examined to search for characteristic differences from those in events without dimuons.

INTRODUCTION

We report the results of an experiment which examined the production of muon-pairs at low mass and low transverse momentum along with the final states accompanying this production.

The experiment is distinguished by its use of a low-momentum (15.5 GeV/c) pion beam, a hydrogen target, and the observation of the entire charged final state. It is sensitive primarily to events with pairs at Feynman $x(x_F)$ greater than 0.3.

The low interaction sensitivity, 8.65 events/nbarn, precluded obtaining statistically relevant data at muon pair masses appreciably above that of the rho.

The observation of the entire event in the streamer chamber allowed excellent mass resolution ($\sim$ 15 MeV FWHM) and a study of the hadrons accompanying the dimuons.

The good mass resolution allowed an examination of the prompt muon pair threshold region and possible "conventional" sources of low-mass muon pairs such as the Dalitz decay of η and ω and dimuon decays of the A_2. None of these account for all of the muon pairs in the low mass region.

APPARATUS

Beam and Target

A beam of 15.5 GeV/c pions was incident on a liquid hydrogen target in the SLAC 2-meter streamer chamber (see Fig. 1 and 2). Photographs were taken in three-camera, 18^o stereo, of triggered events utilizing Kodak S0143 film. Data runs were made with both positive and negative pions. All magnetic fields were reversed when the sign of incident particles was changed, thus preserving the trajectories through the entire

system. Beam intensities of between 2 and 8 pions per pulse at 120 pps were used with the chamber sensitive to the entire pulse. With the one-meter-long 3.2-cm-diameter liquid hydrogen target, the higher intensities led to an average of one interaction per pulse and a large fraction of the photographs contained more than one event.

The liquid hydrogen target had an outer vacuum wall of 0.015 cm of mylar, a thin vacuum insulating region, and an inner liquid container of 0.0076 cm of mylar.[2] Final state protons of momenta less than $\sim$200 MeV/c would not enter the gas of the streamer chamber and would hence be undetected.

On top of the vacuum jacket of the target a foam and acrylic support was attached, serving to strengthen the target assembly and functioning as a delta ray absorber.[2] (Delta rays in the magnetic field of the streamer chamber travel in a tight spiral between the electrodes, and the resulting intense ionization can cause a very bright wide-gap discharge in the streamer chamber that can obscure a portion of the film.) Three fiducials were mounted on top of the support to allow locating the target inside the streamer chamber.

The incident pion beam and interaction vertex are not visible in the streamer chamber, the resulting charged tracks being detected as they leave the target. Therefore, interaction vertices must be reconstructed from the emerging charged tracks.

Streamer Chamber

The central detection device in this experiment was the SLAC two-meter streamer chamber. It was a box two meters long, 0.8 meter wide, and 0.6 meter deep, filled with a 90% neon and 10% helium gas mixture

with one part in 10^3 isobutane (to reduce the voltage necessary for streamer production).

Also contained in the chamber were three planes of wire mesh, forming transparent electrodes. A streamer chamber of this size behaves as a transmission line when a short pulse is applied, and is terminated in its characteristic impedance (34 ohms) to avoid reflections. The chamber was located in a one-meter gap between two circular coils providing a magnetic field of 12.9 kilogauss.

Muon Spectrometer

Data for this experiment were obtained in three runs. Improvements in the apparatus were made for each run, using information from the previous runs. This report primarily describes the arrangement of the final configuration with which two-thirds of the data were obtained.

The muon spectrometer consisted of scintillation counters and magnetostrictive wire chambers, sandwiched in a hadron absorber of copper and lead. There was an opening $\sim$ 9 cm in diameter (indicated by dashed lines in Fig. 1 and 2) in lead and copper walls to allow passage of the unscattered pion beam. Three scintillation counters lay along the path of the unscattered beam and were used to veto events with non-interacting beam pions. The configuration of each of the six planes of scintillation counters is shown in Fig. 3.

The six planes of scintillation counters were arranged in a hodoscope with an effective cell size of $\sim$ 15 $\times$ 15 cm. This was sufficiently small to distinguish muons from pions for all but the very high-momentum tracks. For these high momentum tracks the wire chambers were especially useful.

TRIGGER

The muon spectrometer was used to trigger on events for which the counters indicated that two charged tracks may have penetrated the lead wall. Then offline analysis programs used the spectrometer information along with the measurement of tracks in the streamer chamber picture to determine if two muons were actually produced in the interaction. The detailed method used is described later.

To define the beam, two counters were placed in the beam, and two semi-annular counters were used to veto beam-halo particles. These combined to leave a 3/4" diameter circular hole for the beam.

Three veto counters were placed downstream of the streamer chamber in the beam line. A beam interaction was then defined as a beam particle entering the target and no hit in the downstream veto counters. The veto counters were larger than the beam hole in the lead to reduce false triggers produced by "scraping" of pions. "Scraping" occurred when a fast pion from an interaction in the streamer chamber (elastic scattering, for example) traveled some distance through the beam hole in the lead and then interacted with the lead near the counter banks.

The next step in the trigger used the first two banks of horizontal counters (A and C). At least one hit in the A plane and a correlated hit in the C plane were required.

The vertical planes of counters (B and D) were used to require two possible tracks. The magnetic field in the streamer chamber region separated the positive and negative muons horizontally, and therefore two non-adjacent B hits and, in addition, at least two hits in the D plane were required.

Table I shows the rate at each level of the trigger, the final rate being $\sim$ 2.5 triggers/minute at 180 pps with a pion beam of 8 pions per pulse. This rate was easily handled by the streamer chamber, so no further hardware refinement of the trigger was necessary. However, for analysis purposes, a software trigger with further restrictions was imposed. It required at least one hit in the F plane of horizontal counters in addition to the A and C plane hits required by the hardware trigger. Also, events with more than four hits in the F plane or more than four hits in the B or D vertical planes were interpreted as being due to hadron punchthrough. A minimum separation of B and D plane hits was also required (non-adjacent counters), and the final software restriction was the requirement of at least two sets of correlated B-D hits. That is, a muon passing through a given B-plane counter would pass through a loosely specified region at the D-plane. An acceptance Monte-Carlo calculation indicated that these restrictions had a minimal effect on the dimuon signal.

Calibration data was also taken triggering on interacting particles and on a "1-muon" trigger. The "1-muon" trigger required only one B hit and only one D hit. Both types of calibration data were needed for background calculations and the interaction trigger proved useful for comparison of the data with hadron interactions.

Data reduction proceeded as follows: The events satisfying the software trigger were scanned and events were rejected which did not have at least two tracks with momentum greater than $\sim$ 1.5 GeV/c which could possibly hit the lead wall. In addition, events with one or more of the three reference fiducials obscured and events with greater than

nine positive or nine negative tracks were rejected (rejection rates were less than 2%). In the remaining events, only tracks identified as muon candidates were measured and the resulting measurements reconstructed geometrically by TVGP[3] and the vertex reconstructed by the program APACHE.[4] It should be noted that since the target region was obscured in the streamer chamber, APACHE projected the tracks back into the target and attempted to reconstruct a common vertex.

For each acceptable vertex the momentum vectors for each track were recalculated, using the vertex as a well-measured point on the track. Typical errors for the vertex were 0.3 mm transverse to the beam and magnetic field directions, 1.8 mm parallel to the field direction, and 1.2 mm parallel to the beam direction. The reconstruction of the vertex yielded a longer track length and therefore a better momentum determination for each of the tracks.

The resulting reconstructed tracks and spectrometer information were then used to identify muons. For every vertex each track was extrapolated from the streamer chamber through the spectrometer. At each plane of counters or wire chambers an error was calculated, combining measurement and multiple scattering errors. Correct hits within three standard deviations of this error were required at each plane of counters. The counters that were hit defined a path for the track, and spark chamber positions consistent with the counters were also required to be within three sigma of the extrapolated position. An additional requirement removed events in which tracks of the same charge as the beam hit a group of counters immediately around the beam hole. This cut was made to reduce the number of false muon identifications for pions that

traveled some distance through the beam hole and then interacted in the lead. Each event was checked by physicists for consistency and a final decision made. (This was possible because of the small number of events involved.) Figures 4 and 5 show the horizontal and vertical views of an event. Those events with two identified muons were returned to the measuring table and all tracks in the event were measured. The TVGP and APACHE sequence was then repeated, and the kinematic reconstruction was done by SQUAW.[3,5]

ACCEPTANCE

To determine the dimuon acceptance a Monte Carlo program was run with the hardware and software restrictions described above. The requirement that both muons penetrate the lead to the D-counter level resulted in essentially no acceptance for muon pairs with (x_F) less than 0.3. Therefore, all acceptance numbers, weighted plots, and cross sections quoted refer to dimuon pairs with $x_F > 0.3$.

The Monte Carlo calculation generated muon pairs with uniform distributions in the kinematic variables: mass, x_F, transverse momentum (P_t), and cos θ^* (θ^* is the angle between the muon with charge opposite to that of the beam and the muon pair direction in the rest frame of the muon pair). These events were projected through the spectrometer, and the appropriate counter hits indicated. The momentum vectors and counter data were then used in the same analysis program used to identify muons in the data. The acceptance was calculated as a three-dimensional array in mass, x_F, and cos θ^*, integrating over transverse momentum. For the small values of transverse momentum in this experiment, Monte Carlo studies indicated an acceptance essentially independent

of P_t. Therefore, the experimentally observed P_t distribution, $P_t \cdot \exp(-4.4 \cdot P_t)$ was used in the analysis.

The three-dimensional acceptance array was first integrated over cos θ^*, assuming an isotropic distribution. Events were then weighted as a function of mass and x_F to find the corrected distributions. Using the corrected distributions, the acceptance array was then integrated over mass and x_F to determine the acceptance as a function of cos θ^*. The process was then repeated assuming both $(1 + \cos^2 \theta^*)$ and $\sin^2 \theta^*$ angular distributions. The acceptance in mass and x_F changed by less than 25% for all polarization assumptions. The corrected cos θ^* distribution was best fitted by a flat distribution even when complete polarization was assumed for the acceptance calculation. Therefore, the acceptance in mass and x_F used for weighting distributions and for overall normalization was taken assuming an isotropic angular distribution.

The results of the Monte Carlo calculation are displayed in Fig. 6, showing the acceptance as a function of mass, x_F, and cos θ^*, respectively. The acceptance in dimuon mass is essentially flat over most of the observed range, but the rise shown near threshold is critically dependent on the x_F distribution. Mass plots will be shown uncorrected for acceptance.

NON-PROMPT BACKGROUND

To calculate the hadron contamination remaining in the dimuon sample, use was made of both the "1-muon" and "interaction" triggers described previously. The method used was first to calculate the probability of a hadron of a given momentum simulating a muon by decaying to a muon or penetrating the absorber in our apparatus. These probabilities

were then applied to associated tracks in the "1-muon" events, and a non-prompt background calculated.

To calculate the probabilities, the "1-muon" triggered events were measured and then sent through the same analysis package as the dimuon events. Nine hundred twenty-one acceptable "1-muon" events were found, and their momentum distribution plotted. Approximately 5000 interaction triggers were also measured, and the single-track momentum distributions plotted. By normalizing the interaction triggers to the number of interactions recorded in the "1-muon" sample the number of incident tracks on the lead wall could be obtained, and thus the probability of a single hadron simulating a muon. (This assumes that all of the "1-muon" triggers originated from hadrons. In fact, less than 10% of the "1-muon" triggers are prompt muons. Such a 10% assumption would lead to an overestimate of the background by $\sim$ 1%.) The probabilities obtained are shown in Fig. 7.

Next, each additional track associated with an acceptable "1-muon" trigger was assigned a probability of simulating an additional muon according to its momentum. The results were summed and normalized to the total dimuon sample. Table II shows the results of this calculation, along with statistical errors. The agreement between the calculated and observed like-sign pairs is excellent.

A possible failure of this method would be due to K^+K^- production. The probability of a kaon simulating a muon could be higher than that of a pion, while the calculated probabilities would be a weighted average of the two. Such a contribution can be estimated, using the additional assumptions that at least 50% of the kaon decays would be eliminated as

prompt muon candidates because of the large angle of decay and energy change, and that 3% of all interactions contain K^+K^- pairs. We find that a maximum 1% increase in background would occur, which is within our statistical error.

RESULTS

Inclusive Distributions

From approximately 2.15×10^8 interactions a total of 890 dimuon events were identified, 554 from $\pi^- p$ and 336 from $\pi^+ p$ interactions. Figure 8 shows the raw mass distributions for both beam polarities and the sum of the two. The major features of the distributions are the events in the ρ-ω region and the rise below this region. The features are the same for both beam polarities and therefore for the inclusive analysis the samples will be combined.

Figure 9 shows the transverse momentum distribution, which is well fitted by the form $P_t \cdot \exp(-4.4 \cdot P_t)$ and was used in the acceptance Monte Carlo calculation. In Fig. 10, the cos θ^* distribution is shown. A fit of the form $(1 + A \cos^2 \theta^*)$ was made, resulting in $A = .09 \pm .25$, and a χ^2 of 13 for 18 degrees of freedom.

A beam interaction only trigger was used to compare the dimuon data with dipion data in the same kinematic region. Approximately 5000 events were measured, and then analyzed as dimuon candidates, although all were basically dipions. Appropriate counters were indicated as hit, as if the high-momentum tracks were muons and had penetrated the lead. Those events which satisfied the dimuon criteria were used for comparison with the dimuon sample.

Figure 11 shows the x_F distribution for the dimuon sample compared

to the dipion events. To obtain a single μ/π ratio from our data would require a large extrapolation in x_F. We therefore restrict ourselves to a dimuon/dipion ratio in the kinematic region of this experiment ($x_F > 0.3$). The result is dimuon/dipion = $(5 \pm 2) \cdot 10^{-5}$, essentially constant as a function of x_F. This may be sufficient to account for the observed single μ/π ratio in this region.[6-8]

Another relevant comparison is the dimuon to dipion mass spectrum. A check which makes clear that the dimuon mass spectrum is not merely a reflection of the kinematic cuts imposed by requiring the two muons to penetrate lead, is to compare the dimuon mass spectrum to the dipion mass spectrum (interpreted as muons) in Fig. 12. The number of events in the dipion spectrum are normalized to be the same as in the dimuon plot.

Fits were made to obtain the rho and omega content of the dimuon mass spectrum. With the statistics of this experiment the fits were not very stable with respect to how the data were binned. In an effort to minimize this instability, fits were made to an ideogram of the data (see Fig. 13). For the mass region above 350 MeV, a fit was made to two Breit-Wigner amplitudes (rho and omega) and a background. The background shape was assumed to be a sum of a linear and a Dalitz decay curve ($\eta \to \gamma\mu^+\mu^-$). The fit had five parameters (two for the linear background, one for the Dalitz decay normalization, and one each for the two Breit-Wigner amplitudes) and gave a chi-square of 35 for 46 degrees freedom. The fit gave 105 ± 24 rho events and 60 ± 13 omega events. Fits were also attempted with an interference term assuming a constant relative phase between the rho and omega amplitudes, resulting in essentially the same values for the number of rho and omega events.

The observed data and calculated cross sections for $x_F > 0.3$ are summarized in Table III for both beam polarities and the combined sample. The value of 330 ± 70 nb for $\pi^+ p \to \mu^+\mu^- x$ can be compared with the 340 ± 70 obtained at 150 GeV/c incident pion momentum.[9] The cross section listed in the table for $\pi p \to \eta(x_F > .3) + X$, $\eta \to \mu^+\mu^-$ comes from binning the data in 15 MeV bins centered on the η mass. A statistically very weak signal is then observed at the level shown in the table, (7 ± 5 events). Using the Particle Data Group value[10] of 2.2×10^{-5} for the branching ratio of eta to two muons, a production cross section for eta of 0.4 ± 0.4 mb is obtained assuming an x_F distribution similar to the rho with half of all etas produced having $x_F > 0.3$. The observed value of the eta cross section in this energy region is 1.5 ± 0.3 mb.[11]

Using the Particle Data Group value for $\rho \to \mu^+\mu^-$ decay of $(6.7 \pm 1.2) \times 10^{-5}$ and assuming that ∿ one-half of the rhos are produced with $x_F > 0.3$ as observed in a bubble chamber experiment with $\pi^+ p$ at 16 GeV/c,[12] we obtain a rho inclusive cross section of 2.1 ± 0.9 mb. This can be compared with a value from the same bubble chamber experiment of 4.8 ± 0.4 mb. A similar calculation with respect to ω production, assuming an x_F distribution similar to the rho, yields a 1.1 ± 0.6 mb cross section value. (Here the Particle Data Group value for $\omega \to \mu^+\mu^-$ is derived assuming $\omega \to 2e = \omega \to 2\mu$.)

Final State Distributions

The observation of charged tracks makes possible a comparison of the final state features between dimuon production and other inelastic interactions. In Fig. 14, the charged prong distributions and mean charged multiplicity for dimuon production are shown compared with the

dipion sample described previously. In both the $\pi^+ p$ and $\pi^- p$ plots the muons (or the "muon-like" pions in the dipion events) are not included. We observe no statistically significant difference in prong distributions between dimuon production and other inelastic interactions.

One can also look for associated strangeness in dimuon production. A large fraction of the charged decays of K^o short and lambda are observed as vees in the streamer chamber photographs. Therefore, a large associated strangeness would be observed as a large number of vees in the dimuon events. We observe 22 vees in the 890 dimuon events, which is compatible with the number of vees observed in other streamer chamber experiments, as well as the 2% of events containing vees observed in our dipion sample. In a pi$^-$ nucleon dimuon experiment at 225 GeV/c,[13] the mean charged multiplicity and the number of events containing vees were also observed to be similar to other hadronic interactions.

Figure 15 shows the two- and three-body effective mass of pions accompanying the dimuons. In Fig. 16 and 17, distributions in x_F and P_t of the associated hadrons are shown, comparing dimuon and dipion samples. We observe no difference in the gross features of the hadron final state in dimuon production compared to the previously described dipion production.

We can also look for resonances which decay into charged particles plus a muon pair. In Fig. 18, effective mass distributions are shown for muon pairs plus one or more hadrons. We find no evidence for unknown resonance production as a source of prompt muon pairs.

Low-Mass Pairs

One of the unusual features of the dimuon mass spectrum (Fig. 8) is

the number of muon pairs below the rho mass. A known source of low-mass dimuon pairs is the Dalitz decay of the eta and omega mesons, $\eta \to \mu^+\mu^-\gamma$ and $\omega \to \mu^+\mu^-\pi^o$. The rate and dimuon mass spectra of these decays are calculable by Quantum Electrodynamics, relative to the $\eta \to \gamma\gamma$ and $\omega \to \pi^o\gamma$ rates. Calculations by Lai and Quigg[14] and by Quigg and Jackson[15] show the ratios to be 5.5×10^{-4} for the eta and 9.1×10^{-4} for the omega. Using these calculations[16] and the $\eta \to \mu^+\mu^-$ and $\omega \to \mu^+\mu^-$ signals in the data, we can estimate the Dalitz decay contribution to the dimuon mass spectrum.

First we calculate the eta contribution. The branching ratio for $\eta \to \gamma\gamma$ is 0.38. The ratio $\Gamma(\eta \to \mu\mu\gamma)/\Gamma(\eta \to \gamma\gamma) = 5.5 \times 10^{-4}$; therefore, $B(\eta \to \mu\mu\gamma) = 2.10 \times 10^{-4}$; $B(\eta \to \mu^+\mu^-) = 2.2 \times 10^{-5}$. The calculated acceptance for $(\eta(x_F > 0.3) \to \mu^+\mu^-\gamma)/(\eta(x_F > 0.3) \to \mu^+\mu^-) = 1.0$. Therefore, we should observe $\eta \to \mu\mu\gamma$ at the rate of $9.5 \times \eta \to \mu\mu$. Using the weakly observed $\eta \to \mu\mu$ signal in our data, we would estimate a contribution of 67 dimuon events from the Dalitz decay of the eta.

Similarly for the omega, $B(\omega \to \pi^o\gamma) = 0.088$, and $\Gamma(\omega \to \mu\mu\pi^o)/\Gamma(\omega \to \pi^o\gamma) = 9.1 \times 10^{-4}$. This yields $B(\omega \to \mu\mu\pi^o) = 8.11 \times 10^{-5}$, while $B(\omega \to \mu\mu) = 7.6 \times 10^{-5}$. For the omega decays the ratio of acceptances is 0.55, and, therefore, we should observe $\omega \to \mu\mu\pi^o$ at the rate of $0.59 \times$ the observed $\omega \to \mu\mu$ signal. This leads to an estimate of 35 dimuon events from the Dalitz decay of the omega.

Figure 19 shows the dimuon spectrum (background subtracted) with the estimate for the sum of the eta and omega Dalitz decays. This estimate is clearly insufficient to account for the low-mass dimuon signal. The method used eliminates systematic normalization errors, giving a

self-consistent estimate. However, there are large uncertainties in the omega and eta to two muon branching ratios, and the eta to two muon signal is very weak in our data. But even with these uncertainties, there appears to be a signal not attributable to the Dalitz decays, since the shape of the Dalitz decay spectrum is different from the low mass spectrum observed.

To show this difference, a maximum Dalitz decay contribution is calculated. For this calculation, equal contributions from the eta and the omega Dalitz decays are assumed, and the resulting spectrum is normalized to the threshold region in the dimuon spectrum. This is equivalent to assuming a 0.8 mb inclusive eta cross section and a 3.6 mb inclusive omega cross section (much larger than is consistent with our $\omega \rightarrow \mu\mu$ signal). The results of this calculation are shown in Fig. 20, where it is seen that even with an extremely large Dalitz decay signal, there still remains another source of low-mass dimuon pairs.

Other mesons (rho, eta', phi, etc.) have radiative decays, and the dimuon spectrum from the higher-mass decays does have a slightly higher average mass, so in principle these decays could broaden the Dalitz decay spectrum and account for the low-mass signal. However, either the production cross section or the branching ratios for these decays are extremely small compared to the eta and omega, and estimates of their contribution to our dimuon mass spectrum are negligible (< 2 events). The two-step Bethe-Heitler production of dimuons makes a negligible contribution because of the use of a hydrogen target.

To investigate differences in production of low-mass pairs from production of dimuons in the rho-omega resonance region, we divide the data into two parts: $M_{\mu\mu} < 600$ MeV and $M_{\mu\mu} > 600$ MeV. Figures 21-23

show the P_t, cos θ^*, and x_F distributions for these two mass regions. The P_t distributions are similar, and the cos θ^* distributions are statistically the same, although our acceptance in cos θ^* for the rho-omega region does not cover a large enough range to give much information. However, the x_F distributions are clearly different, with the low mass region being steeper. Linear fits to two regions result in slopes of (-5.21 ± 0.31) per unit of x_F for the low-mass region and (-3.5 ± 0.4) per unit of x_F for the rho-omega region. This is in agreement with other πp experiments,[17] where the x_F distribution was also observed to be steeper at lower masses.

In Fig. 24 and 25 the P_t and x_F of the final state hadron distributions are compared for the two mass regions and no statistically significant differences are observed. In Fig. 26 and 27 some effective mass combinations are shown for the two dimuon mass regions. Again we find no evidence for mu-mu-hadron decays of resonances as a source of muon pairs.

Exclusive Channels

For exclusive channel information, we rely on the 4-C and 1-C fits from the SQUAW kinematic fitting program. However, the small number of events from these fits makes obtaining statistically meaningful information very difficult. In bubble chamber experiments at this energy,[11] approximately 10% of the interactions make 4-C fits (no neutral particles in the final state). Known losses in the streamer chamber due to vertex reconstruction and slow protons not leaving the target reduce this number by $\sim$ 20%. In principle, the requirement of two high-momentum tracks in the interaction could change this fraction dramatically. As a check, using the limited statistics of our dipion sample we find $(7 \pm 1.5)\%$ 4-C

events. In the dimuon sample 6.3% of the fully measured dimuon events are reconstructed as 4-C events. The dimuon mass spectrum from the 4-C fits is shown in Fig. 28. We see no evidence for a low-mass enhancement in the sample containing an all charged particle final state. This may be an indication that the low-mass muon pairs are produced preferentially in association with one or more neutral particles.

The I-C fits (one missing neutral particle) are contaminated somewhat by events with two or more neutral particles. In Fig. 29-31 the dimuon and mu-mu-neutral mass spectra are shown for the 1-C fits. The mu-mu-gamma and the mu-mu-pi^o mass spectra are interesting in that one may look for evidence of the Dalitz decays of the eta and omega mesons, $\eta \to \mu^+\mu^-\gamma$, and $\omega \to \mu^+\mu^-\pi^o$. We find, however, no evidence for omega, eta, or any other resonance in the mu-mu-neutral mass plots.

A plot of the dimuon mass versus missing mass squared is shown in Fig. 32. There is an accumulation of events in the rho-omega region with small values of missing mass, while no such correlation is observed in the low-mass region. In Fig. 33 the dimuon spectrum is shown from all events making either a 4-C or 1-C fit. The inclusive spectrum is shown on the same figure, normalized to the rho-omega region. The two spectra are clearly different in the low-mass region. The percentages of the total number of events with mass less than 510 MeV are:

Inclusive spectrum - (46.9 ± 1.7)%

4-C spectrum - (21.3 ± 6.0)%

All fits - (28.7 ± 3.5)%

Since the low mass enhancement is not explained by Dalitz decays and is not observed in either the 4C or 1C fits, more neutral particles must be

produced in association with the low mass muon pairs than in the rho-omega region.

MODELS

A paper by Dunbar[18] suggests that tensor meson decay could account for the low-mass signal. In particular, this calculation shows that the $f \to \rho\, \mu^+\mu^-$ and the $A_2 \to \rho\, \mu^+\mu^-$ would produce a dimuon spectrum similar to that observed, assuming equal contribution from both decays. The magnitude of the signal is estimated to be approximately equal to the rho to two-muon signal, assuming no difference in experimental acceptance.

However, the decays of the f and A_2 mesons are unlikely to be a large source of muon pairs in our experiment. If the f and A_2 have x_F distributions similar to the rho, the acceptance of our apparatus for muon pairs from these decays would be approximately a factor of 2.5 less than that for the rho. Also the decay $f \to \rho\, \mu^+\mu^-$, $\rho \to \pi^\pm\pi^-$ contains all charged tracks which are observed in the streamer chamber. Therefore, to look for evidence of this decay, in Fig. 34, the effective mass of the $\pi^+\pi^-\mu^+\mu^-$ system is plotted for $M_{\mu^+\mu^-} < 550$ MeV and 660 MeV $< M_{\pi^+\pi^-} <$ 880 MeV. The arrow points to the mass of the f(1270 MeV). From this plot, it can be seen that $f \to \rho\, \mu^+\mu^-$ is not a large source of dimuons in this experiment.

The $A_2 \to \omega\, \mu^+\mu^-$ decay will usually involve an undetected π^o, since the dominant decay of the omega is $\pi^+\pi^-\pi^o$. We can, however, obtain an upper limit on the number of events from this 5-body decay, since the effective mass of the four charged particles from this decay must be $< (M_{A_2} - M_{\pi^o})$. In Fig. 35 the effective mass of $\pi^+\pi^-\ \mu^+\mu^-$ is shown for

$M_{\pi^+\pi^-} < 650$ MeV, $(M_\omega - M_{\pi^0})$, and $M_{\mu^+\mu^-} < 550$ MeV. There are 51 events with $M_{\pi^+\pi^-\mu^+\mu^-} < 1175$ MeV, which is certainly an upper limit on the number of dimuon events from this decay of the A_2. Any reasonable background curve would leave very few candidates, and the $A_2 \to \omega\, \mu^+\mu^-$ is, therefore, unlikely to be a primary source of dimuons in this experiment.

A purely phenomenological cluster model by Gurtu et al.[19] produces a rise at threshold similar to that observed while a more detailed prediction by Craigie and Schildknecht[20] suggests that the rho may have a low-mass tail into two muons, due to the photon propagator dependence on q^2. The paper points out that the narrow resonance approximation to dilepton production by vector mesons, which assumes a production amplitude multiplied by a constant branching ratio, does not take into account the $1/q^2$ vector meson photon coupling. The dimuon mass spectrum due to rho and omega mesons is calculated with the photon propagator included.

Figure 36 shows such a calculation superimposed on the dimuon spectrum. The calculation fits the mass spectrum very well. However, the fact that there are apparently more neutral particles in the low-mass region and that the x_F distribution of the low-mass pairs appears to be steeper than that of the rho-omega region may be difficult to explain in such a context.

Other theoretical suggestions have been made of possible low-mass enhancements involving parton-parton, pion-parton, and pion-pion annihilation.[21-24] In particular, bremsstrahlung-type interactions as suggested by Farrar and Frautschi[22] would have a threshold-type enhancement similar to that of the Dalitz decay spectrum, and would also predict a large number of real photons.

A calculation of a more general nature[24] using the framework set up by Sachrajda and Blankenbecler[21] results in a mass spectrum similar to that observed in the low-mass region (Fig. 37). The calculation involves pion-pion annihilation, and the pion form factor plays a major role. Since the pion form factor is dominated by the rho, this calculation becomes very similar to the Craigie and Schildknecht model.

A suggestion by Bjorken and Weisberg[23] is that "wee quarks" may account for a higher dilepton rate than predicted by the Drell-Yan[25] mechanism. That is, quarks and anti-quarks produced during the interaction process (to produce the observed hadrons) may also annihilate to produce lepton pairs, and a rate of $\sim$ 25 is gained over the normal Drell-Yan process. It is suggested that this type of mechanism would produce an enhancement peaking below the rho mass. However, no specific shape is estimated.

SUMMARY

A clear, prompt dimuon signal has been observed in a streamer chamber experiment with 15.5 GeV/c pi p interactions. The dimuon mass spectrum exhibits a low-mass enhancement, along with the dimuon decays of the rho and omega mesons. Estimates of muon pairs from the Dalitz decays of the eta and omega mesons are inadequate to account for the low-mass region. Also, the shape of the calculated Dalitz spectrum (independent of normalization) is shown not to fit the data in this region. Theoretical suggestions concerning sources of low-mass dimuons are discussed, and two calculations give excellent agreement with the shape of the mass spectrum data. These calculations may have difficulty in accounting for final state differences in the rho and lower mass region

and an x_F difference of the dimuons in these two regions.

This experiment is unique in that the charged final state is observed. In the absence of detailed models, general features of the charged hadrons are presented and compared to a sample of interactions containing pion pairs kinematically similar to the muon pairs. The general features of the inclusive charged final state in interactions producing prompt muon pairs appear to be very similar to a kinematically similar sample of hadronic interactions, yielding little information as to the origin of the low-mass muon pairs.

The exclusive (fitted) final states show an excess of neutral particles produced in association with the low-mass muon pairs. It is possible that this is a result of a large Dalitz decay contribution. However, this would necessitate production mechanisms of the eta and omega mesons such that their Dalitz decays would not be observed in our 1-C fits.

ACKNOWLEDGMENTS

We would like to acknowledge the assistance given us by the SLAC accelerator and scanning and measuring staffs. We have received major assistance also from V. Lee, E. McNerney, J. Moss, F. Plunder, T. Pulliam, L. Schwarcz, F. Shuster, and W. Wadley of the streamer chamber operating group.

REFERENCES

1. K. Bunnell et al., Phys. Rev. Lett. 40, 136 (1978).
2. A. Seiden, Ph.D. Dissertation, Univ. of Calif., Santa Cruz (1974).
3. T. B. Day, TVGP SQUAW Operational Information, Tech. Report #649, U. of Maryland, Dept. of Physics & Astronomy, AEC-ORD-2504-100.
4. Margaret Garnjost, Lawrence Berkeley Laboratory, Group A, Programming Memorandum, P. 239 (private communication.
5. O. I. Dahl, T. B. Day, F. T. Solmitz, SQUAW Kinematic Fitting Program, UCRL-AGM-P-126 (Aug. 1965).
6. L. B. Leipuner et al., Phys. Rev. Lett. 35, 1613 (1975).
7. H. Kasha et al., Phys. Rev. Lett. 36, 1007 (1976).
8. D. Buchholz et al., Phys. Rev. Lett. 36, 932 (1976).
9. K. J. Anderson et al., Phys. Rev. Lett. 37, 799 (1976).
10. Particle Data Group, Phys. Lett. 75B, 1-250 (1978).
11. J. Bartke et al., Nucl. Phys. B118, 360 (1977).
12. J. Bartke et al., Nucl. Phys. B107, 93 (1976).
13. Johckheere et al., Phys. Rev. D16, 2073 (1977).
14. C. H. Lai and C. Quigg, FNAL Report No. FN-296 (1976), (unpublished).
15. C. Quigg and J. D. Jackson, Univ. of Calif. Radiation Laboratory Report No. UCRL-18487 (1968), (unpublished).
16. Recent measurements confirm the basic accuracy of the theoretical calculations, Yu B. Bushnin et al., Phys. Lett. 79B, 147 (1978). R. I. Dzhelyadin et al., Phys. Lett. 84B, 143 (1979).
17. J. Alspector et al., "Muon Pair Production by 16 GeV Pions," UR-617 (1977); S. V. Golovkin et al., Sov. J. Nucl. Phys. 30(2), 198 (1979).
18. I. H. Dunbar, Phys. Rev. Lett. 41, 210 (1978).

19. A. Gurtu, D. S. Narayan, and K. V.L. Sarma, Phys. Lett. 64B, 329 (1976).

20. N. S. Craigie and D. Schildknecht, Nucl. Phys. B118, 311 (1977).

21. C. T. Sachrajda and R. Blankenbecler, Phys. Rev. D12, 3624 (1975).

22. G. R. Farrar and S. C. Frautschi, Phys. Rev. Lett. 36, 1017 (1976).

23. J. D. Bjorken and H. Weisberg, Phys. Rev. D13, 1405 (1976).

24. T. Goldman, M. Duong-van, and R. Blankenbecler, "Low Mass Lepton Pairs from Hadron and Neutrino Beams," SLAC-PUB-2283 (1979).

25. S. D. Drell and T. M. Yan, Phys. Rev. Lett. 25, 316 (1970).

TABLE I

Data Reduction Rates

Level of Trigger	Number of Events	Rate per Interaction
Incident Pions	2.2×10^{9}	10
Observed Beam Interactions	1.7×10^{8}	0.78
Correlated A.C. Trigger	6.6×10^{6}	3×10^{-2}
Master Trigger	6.6×10^{4}	3×10^{-4}
Software Trigger	1.2×10^{4}	5.5×10^{-5}
Dimuon Events	890	4×10^{-6}

TABLE II

RESULTS OF BACKGROUND CALCULATION

π^+ P

Charge of Muons	Observed Events	Calculated Background
+ +	26	25.5 ± 4.8
- -	2	3.1 ± 1.6
+ -	336	50.4 ± 5.2

π^- P

Charge of Muons	Observed Events	Calculated Background
+ +	9	8.4 ± 3.5
- -	42	40.7 ± 7.9
+ -	554	98.2 ± 10.8

TOTAL

Charge of Muons	Observed Events	Calculated Background
+ +	35	33.9 ± 5.9
- -	44	43.8 ± 8.1
+ -	890	148.6 ± 12.0

TABLE III

INCLUSIVE CROSS SECTIONS

	π^+	π^-	Combined
Interactions	99×10^6	117×10^6	215×10^6
Sensitivity (ev/nb)	4.12	4.53	8.65
Dimuons found (background)			
$\mu^+ \mu^-$	336 (50)	554 (98)	890 (149)
$\mu^+ \mu^+$	26 (26)	9 (8)	35 (34)
$\mu^- \mu^-$	2 (3)	42 (41)	44 (44)
Cross Section Observed $x_F > 0.3$ (nb)			
$\pi p \to \mu^+ \mu^- X$	330 ± 70	480 ± 100	410 ± 90
$\pi p \to \rho X \to \mu^+ \mu^- X$			62 ± 21
$\pi p \to \omega X \to \mu^+ \mu^- X$			35 ± 12
$\pi p \to \eta X \to \mu^+ \mu^- X$			4 ± 3

$(\pi^- p \to \mu^+\mu^- X)/(\pi^+ p \to \mu^+\mu^- X) = 1.46 \pm .27$

$(\pi p \to \mu^+ \mu^- X)/(\pi p \to \pi^+\pi^- X) = (5 \pm 2) \times 10^{-5}$

FIGURE CAPTIONS

1. Plan View of Apparatus.
2. Side View of Apparatus.
3. Counter Configuration.
4. Horizontal View of Visual Display Generated by the Muon Tracking Program.
5. Vertical View of Visual Display.
6. Acceptance for Prompt Muon Pairs.
7. Experimental Probability of a Hadron Simulating a Muon in Our Apparatus. (Solid line represents the probability of decay.)
8. Dimuon Mass Spectrum: (a) $\pi^+ p \to \mu\mu X$;
   (b) $\pi^- p \to \mu\mu X$;
   (c) combined sample.
9. Transverse Momentum of Muon Pairs.
10. Decay Angle of Muon Pairs in Helicity Frame.
11. Feynman x of Muon Pairs Compared to Pion Pairs (pion pairs multiplied by 10^{-4}).
12. Mass Spectrum of Muon Pairs Compared to Pion Pairs.
13. Ideogram of Dimuon Mass Spectrum.
14. Prong Distributions Comparing Dimuon and Dipion Events.
15. Effective Mass of Associated Hadrons:
   (a) $M(\pi^+\pi^+\pi^-)$;
   (b) $M(\pi^+\pi^-\pi^-)$;
   (c) $M(\pi^+\pi^-)$.
16. Feynman x of Associated Hadrons.
17. Transverse Momentum of Associated Hadrons.
18. Effective Mass of Muon Pairs with Associated Hadrons:
   (a) $M(\mu^+\mu^-\pi^+)$;
   (b) $M(\mu^+\mu^-\pi^-)$;
   (c) $M(\mu^+\mu^-\pi^+\pi^-)$.
19. Dimuon Mass Spectrum with Estimate of Dalitz Decay Contribution.
20. Dimuon Mass Spectrum with Maximum Dalitz Decay Contribution.
21. Transverse Momentum of Muon Pairs in Two Dimuon Mass Regions.
22. Decay angle of Muon Pairs in Two Dimuon Mass Regions.

FIGURE CAPTIONS

23. Feynman x of Muon Pairs in Two Dimuon Mass Regions.

24. Transverse Momentum of Associated Hadrons in Two Dimuon Mass Regions.

25. Feynman x of Associated Hadrons in Two Dimuon Mass Regions.

26. Effective Mass of Associated Hadrons in Two Dimuon Mass Regions.
    (a) $M(\pi^+\pi^-)$ with $M(\mu^+\mu^-) < 600$ MeV.
    (b) $M(\pi^+\pi^-)$ with $M(\mu^+\mu^-) > 600$ MeV.
    (c) $M(\pi^+\pi^-\pi^+)$ with $M(\mu^+\mu^-) < 600$ MeV.
    (d) $M(\pi^+\pi^-\pi^+)$ with $M(\mu^+\mu^-) > 600$ MeV.

27. Effective Mass of Muon Pairs with Associated Hadrons in Two Dimuon Mass Regions.
    (a) $M(\mu^+\mu^-\pi^\pm)$ with $M(\mu^+\mu^-) < 600$ MeV.
    (b) $M(\mu^+\mu^-\pi^\pm)$ with $M(\mu^+\mu^-) > 600$ MeV.
    (c) $M(\mu^+\mu^-\pi^+\pi^-)$ with $M(\mu^+\mu^-) < 600$ MeV.
    (d) $M(\mu^+\mu^-\pi^+\pi^-)$ with $M(\mu^+\mu^-) > 600$ MeV.

28. Dimuon Mass Spectrum for Events Making a 4-C Fit. (Inclusive spectrum is normalized to the ρ region.)

29. Mass Spectrum for Events Making a Gamma Fit:
    (a) $M(\mu^+\mu^-)$;
    (b) $M(\mu^+\mu^-\gamma)$;

30. Mass Spectrum for Events Making a π^o Fit.
    (a) $M(\mu^+\mu^-)$
    (b) $M(\mu^+\mu^-\pi^o)$

31. Dimuon Mass Spectrum for Events Making a Neutron Fit.

32. Dimuon Mass vs. Missing Mass Squared.

33. Dimuon Mass Spectrum from Events Making any 4-C or 1-C Fit. (Inclusive spectrum is normalized to the ρ region.)

34. Effective Mass of $\mu^+\mu^-\pi^+\pi^-$, Searching for f-Meson.

35. Effective Mass of $\mu^+\mu^-\pi^+\pi^-$, Searching for A_2-Meson.

36. Dimuon Mass Spectrum with Calculation by Craigie and Schildknecht.[20]

37. Dimuon Mass Spectrum with Calculation by Goldman *et al.*[24]

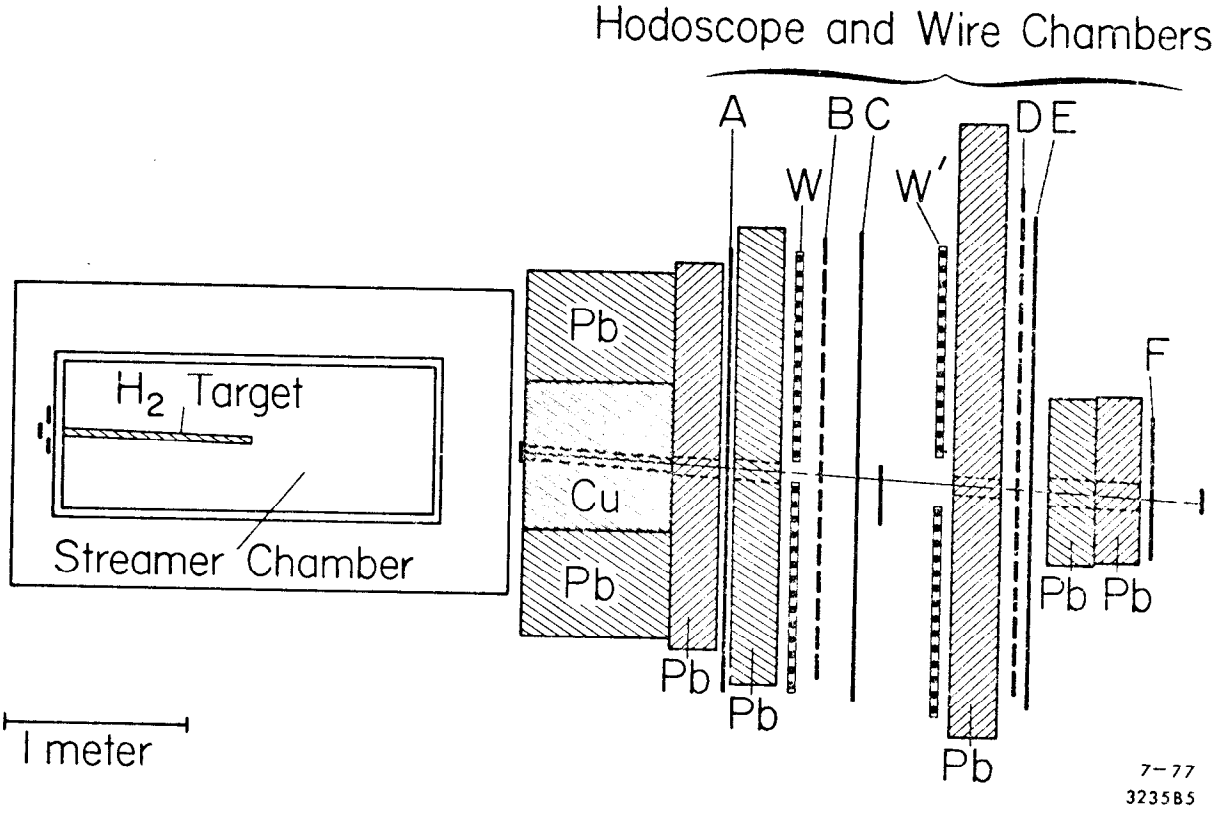
Hodoscope and Wire Chambers
A
B C
D E
W
W'
F
Pb
Cu
Pb
H_2 Target
Streamer Chamber
Pb
Pb
Pb
Pb
Pb
1 meter
7-77
3235B5

Fig. 1

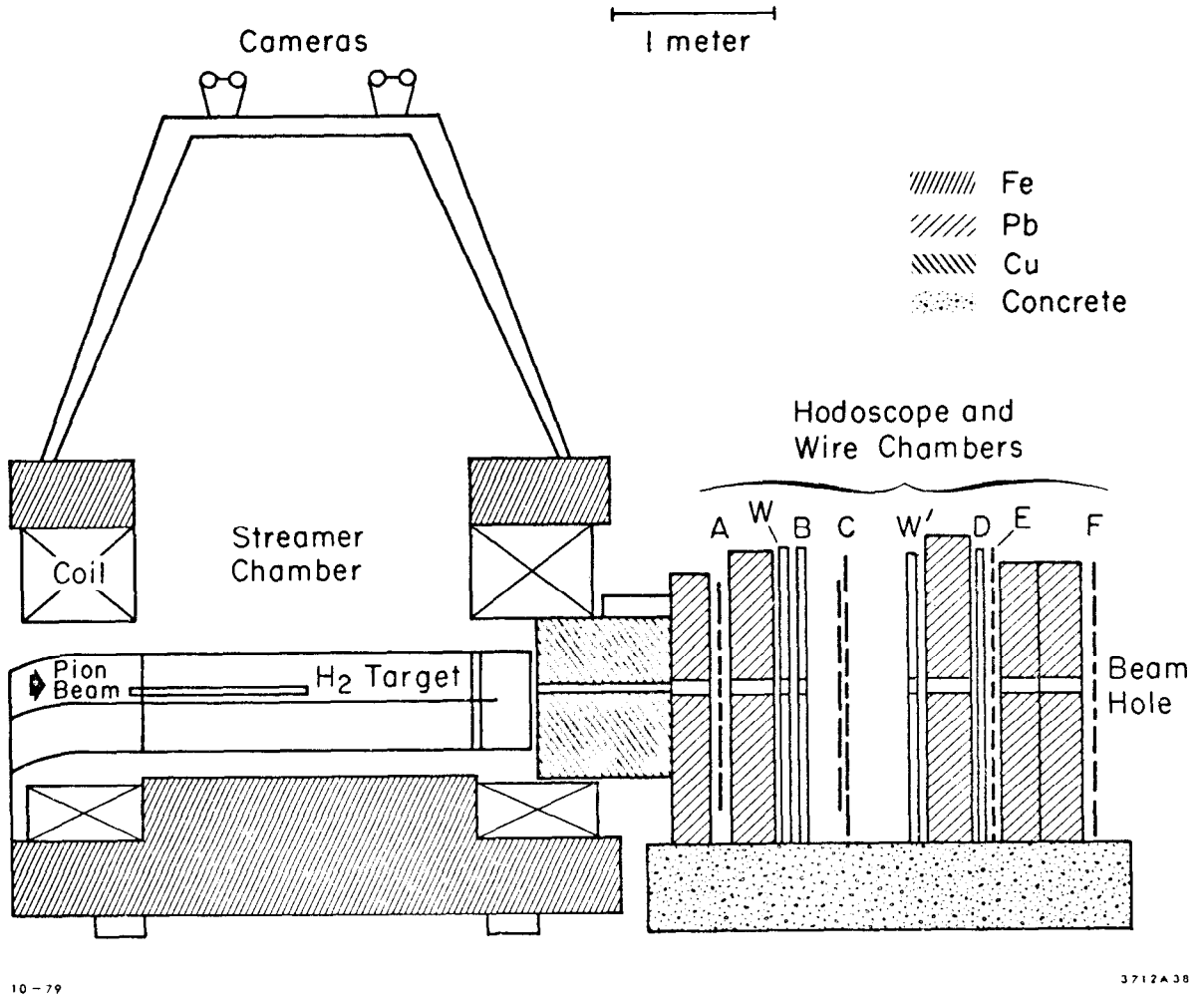
Cameras
1 meter
Fe
Pb
Cu
Concrete
Hodoscope and
Wire Chambers
A
W
B
C
W'
D
E
F
Coil
Streamer
Chamber
Pion
Beam
H_2 Target
Beam
Hole
10-79
3712A38

Fig. 2

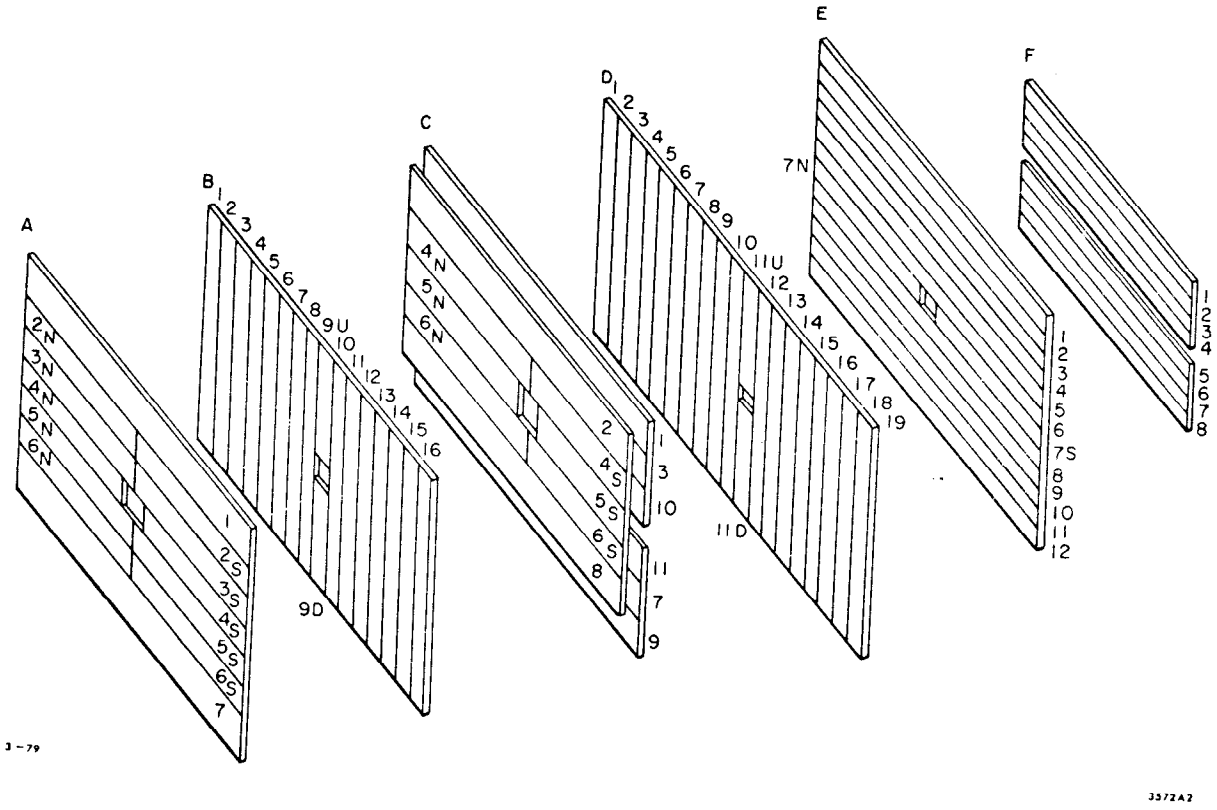

Fig. 3

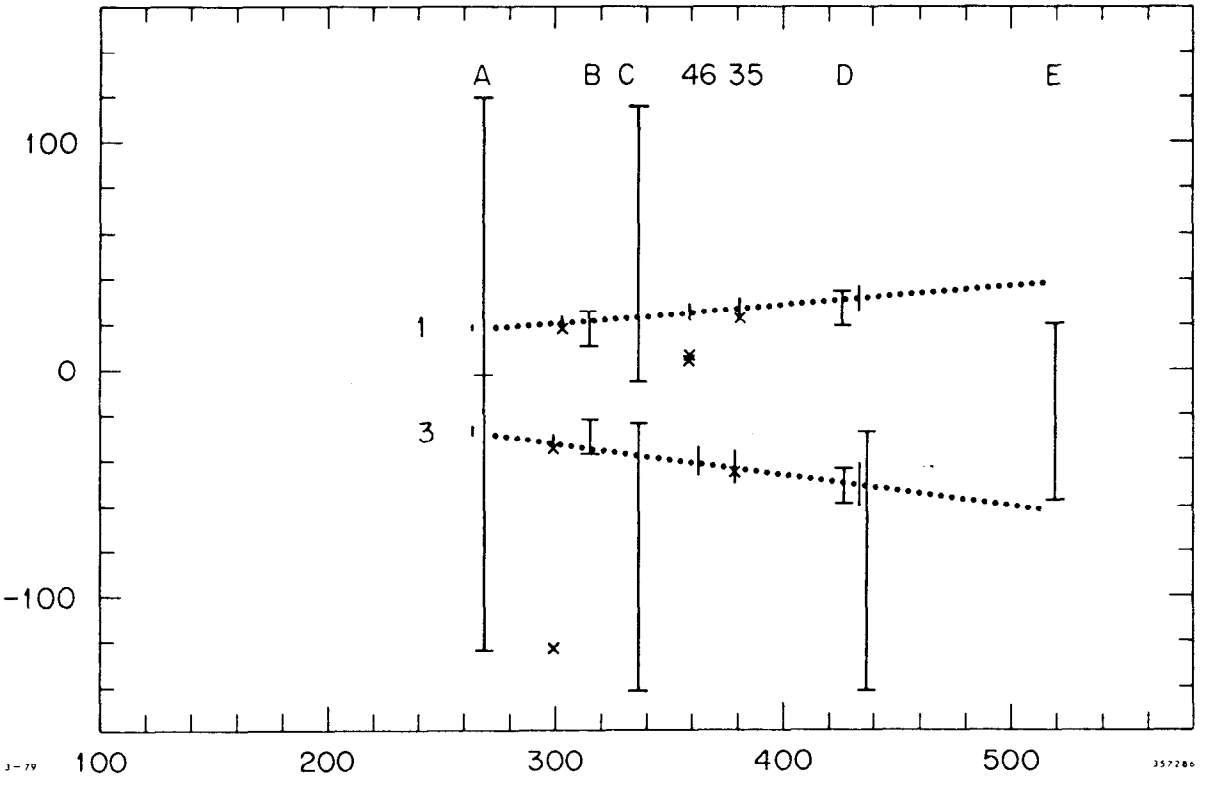

Fig. 4

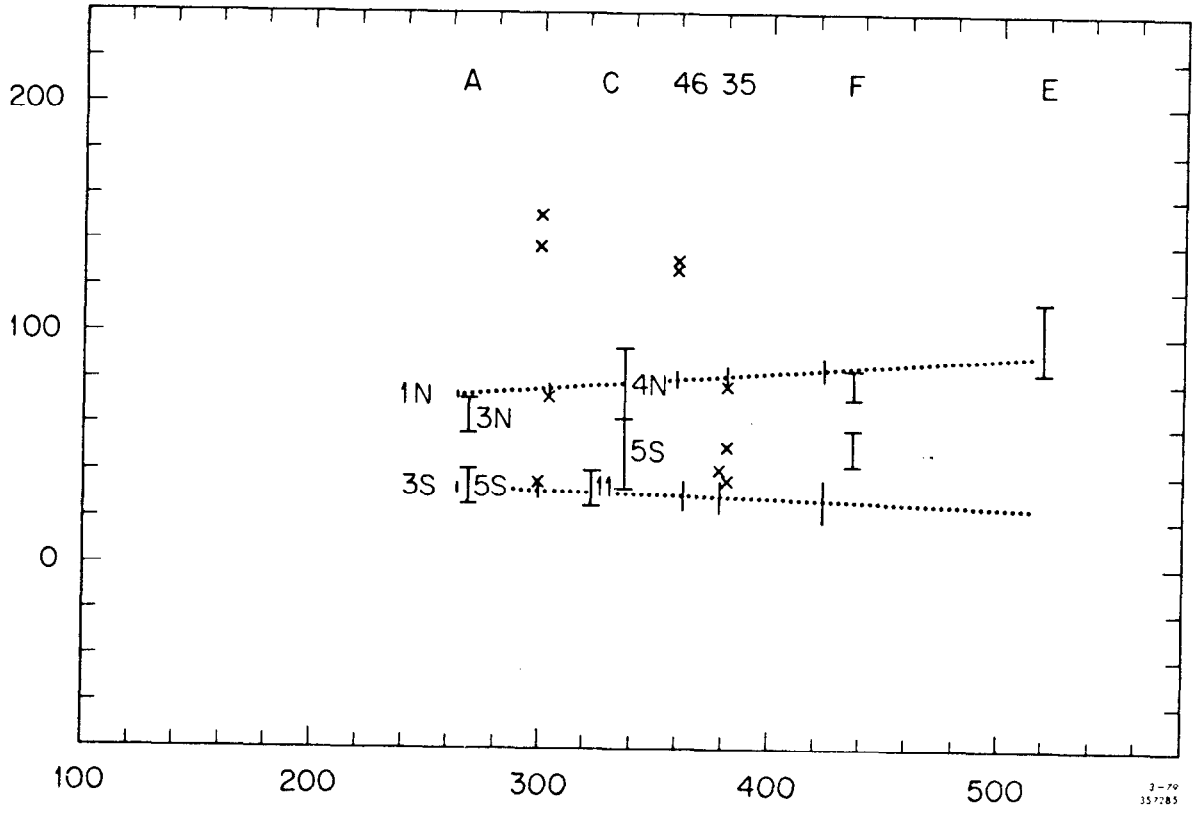

Fig. 5

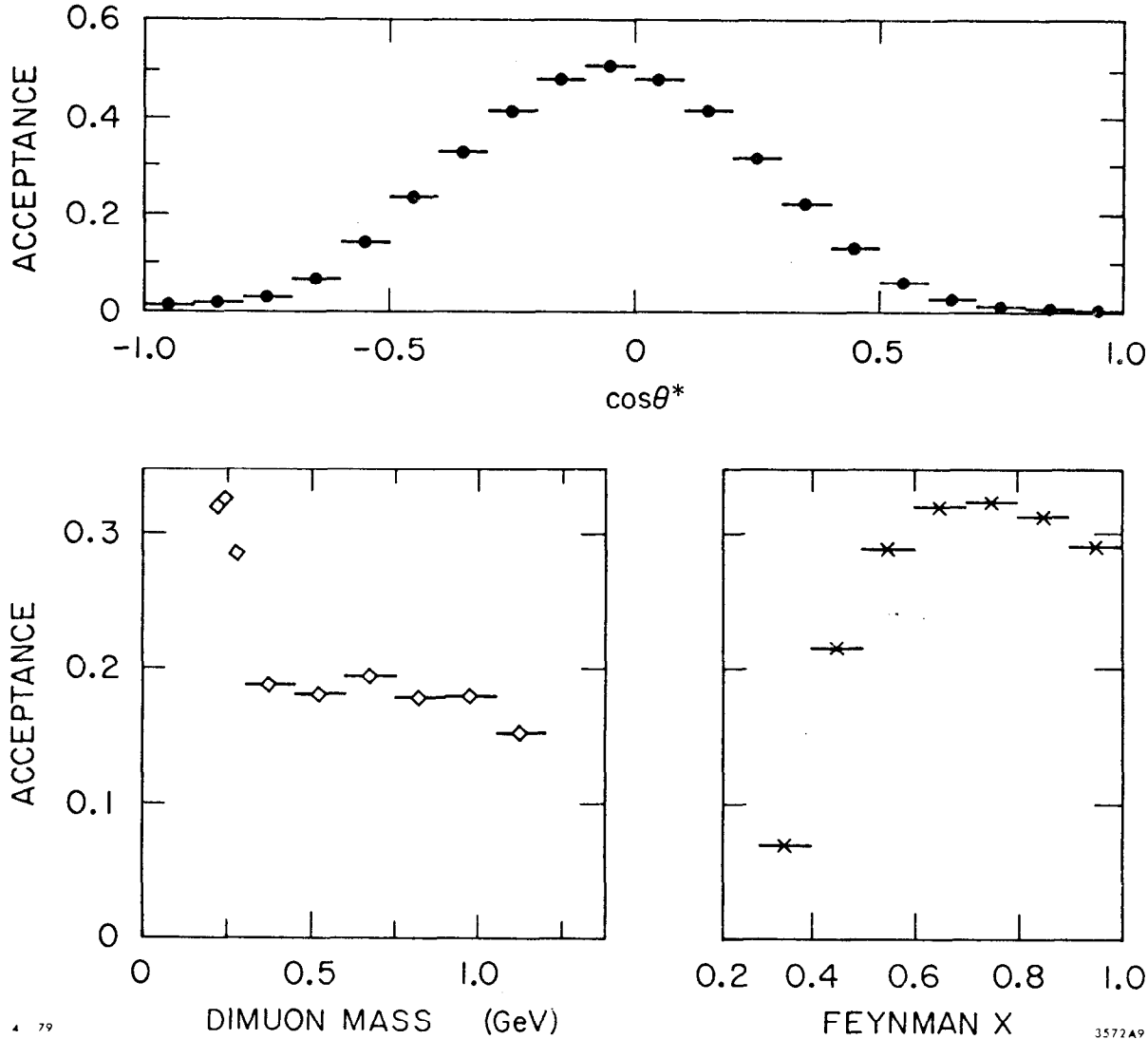
ACCEPTANCE
0.6
0.4
0.2
0
-1.0
-0.5
0
0.5
1.0
cosθ*
ACCEPTANCE
0.3
0.2
0.1
0
0
0.5
1.0
DIMUON MASS (GeV)
0.2
0.4
0.6
0.8
1.0
FEYNMAN X
3572A9

Fig. 6

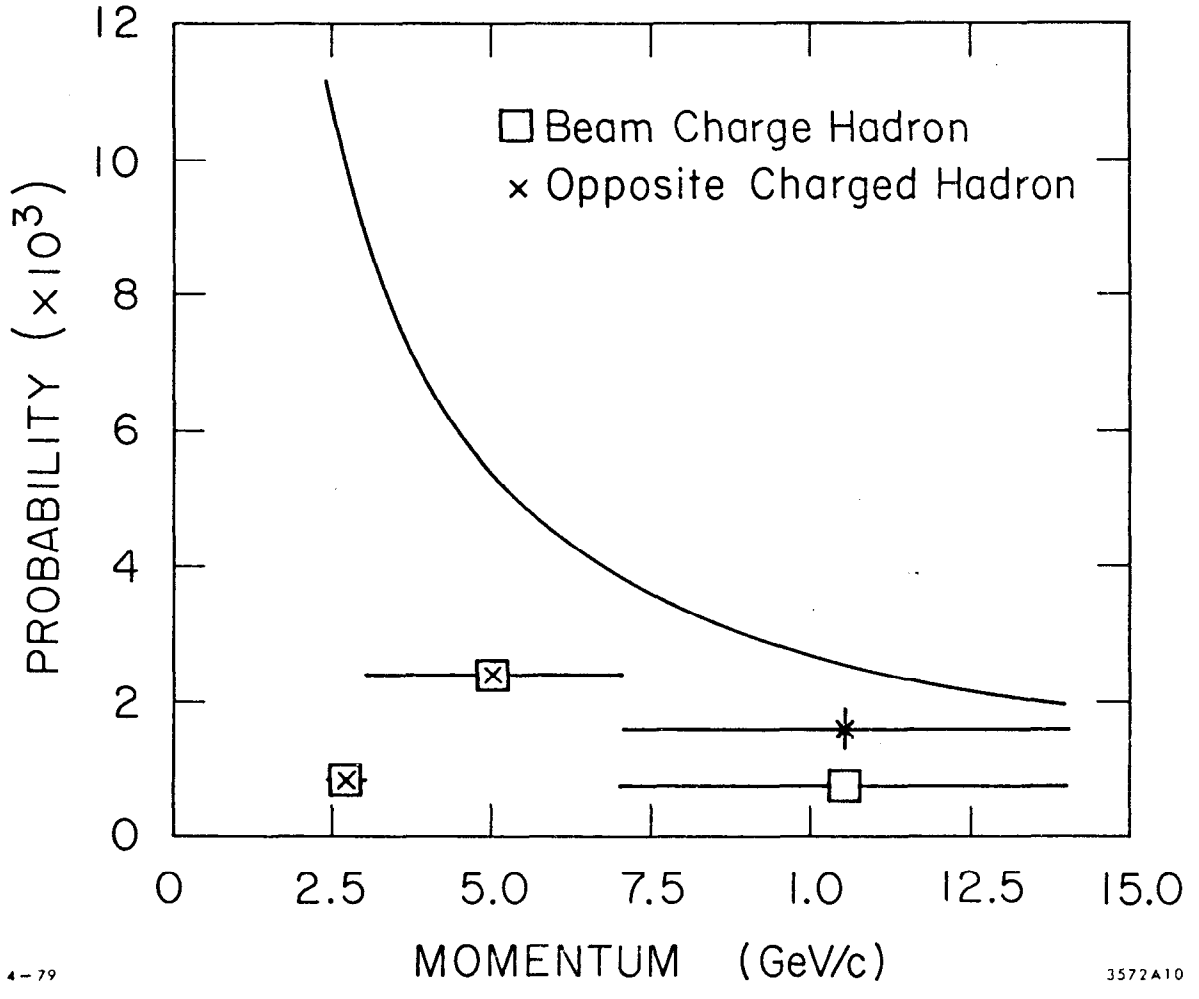
12
10
8
6
4
2
0
PROBABILITY (×10³)
□ Beam Charge Hadron
× Opposite Charged Hadron
0
2.5
5.0
7.5
1.0
12.5
15.0
MOMENTUM (GeV/c)
4-79
3572A10

Fig. 7

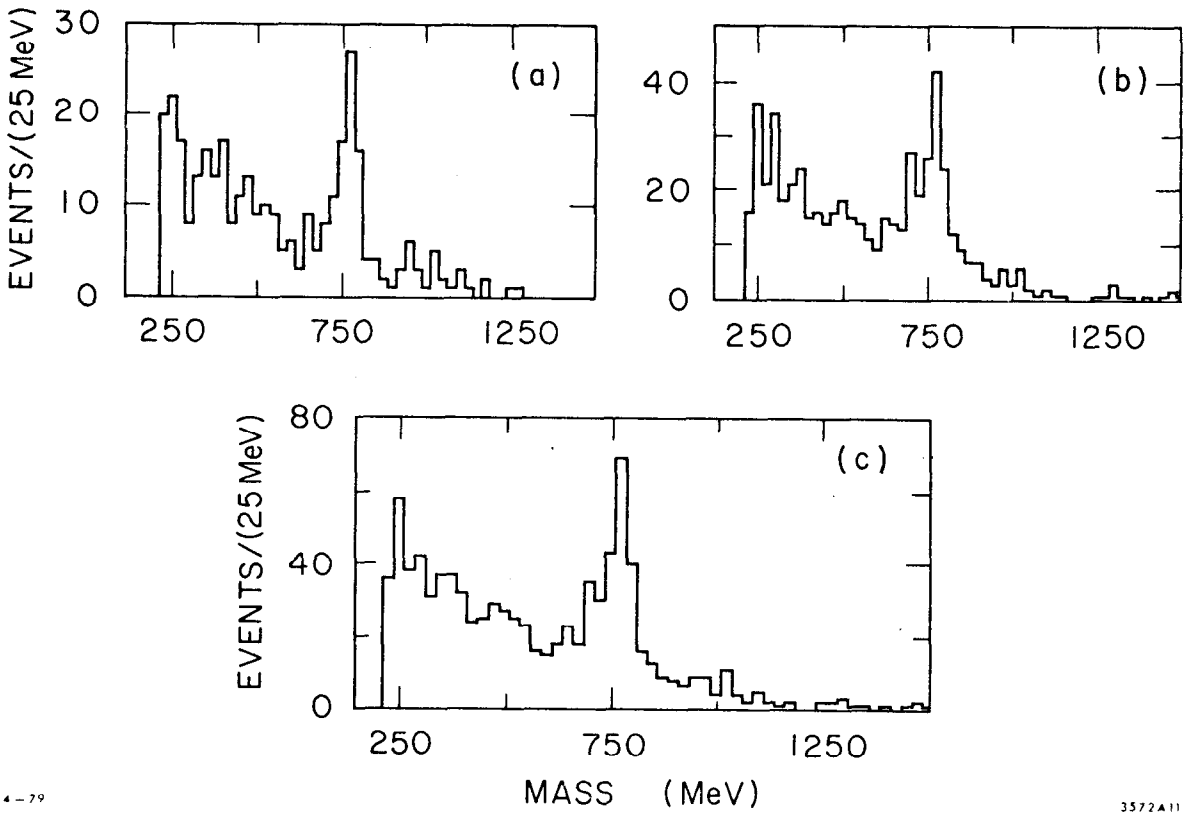
EVENTS/(25 MeV)
30
20
10
0
(a)
250
750
1250
40
20
0
(b)
250
750
1250
80
40
0
(c)
250
750
1250
MASS (MeV)
4-79
3572A11

Fig. 8

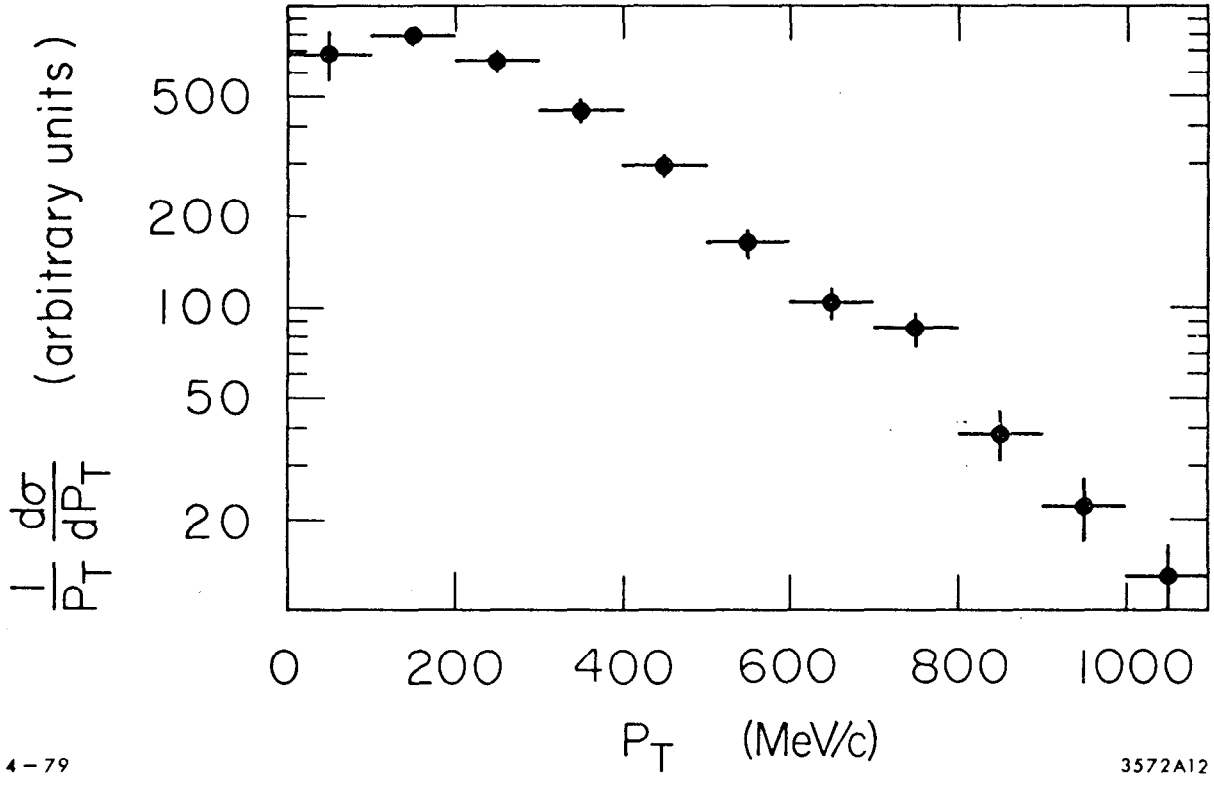
$\frac{1}{P_T}\frac{d\sigma}{dP_T}$ (arbitrary units)
500
200
100
50
20
0
200
400
600
800
1000
P_T (MeV/c)
4 – 79
3572A12

Fig. 9

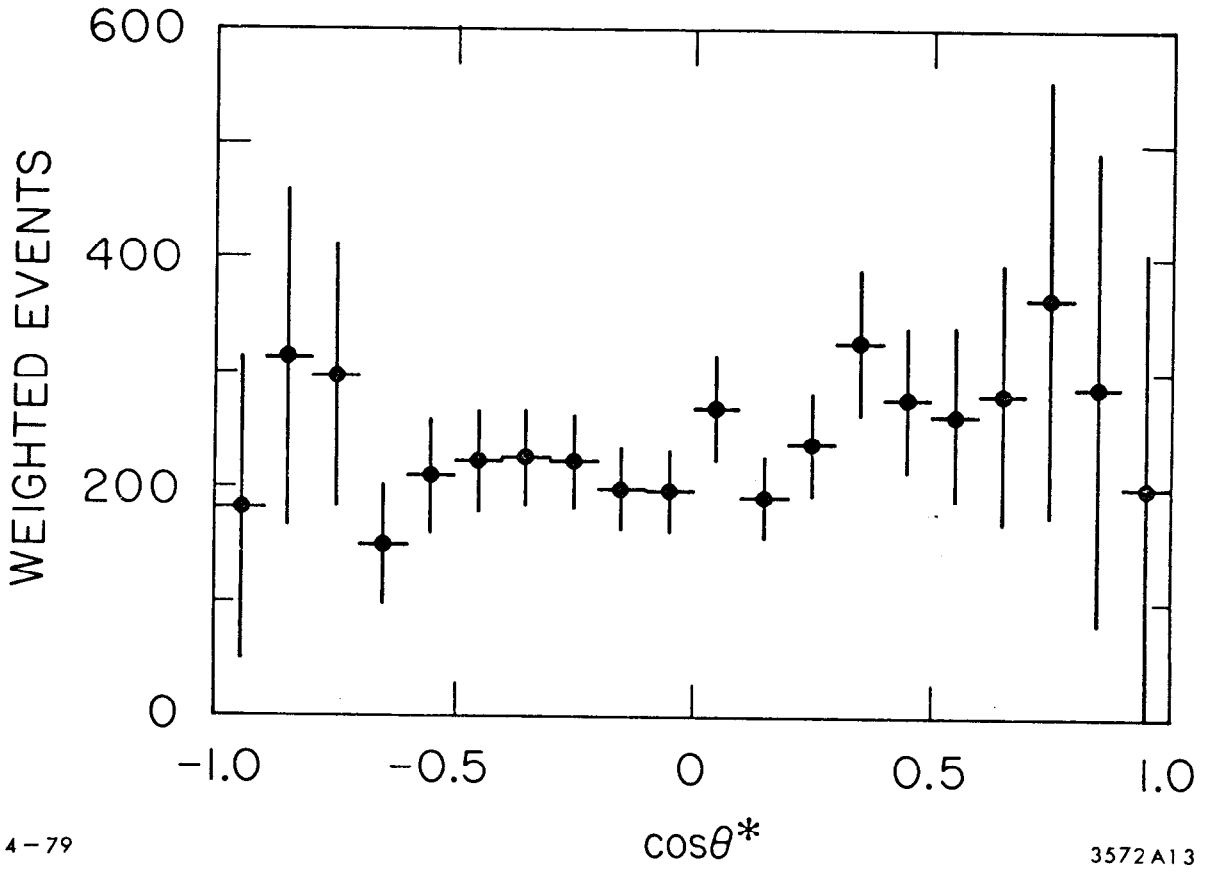

Fig. 10

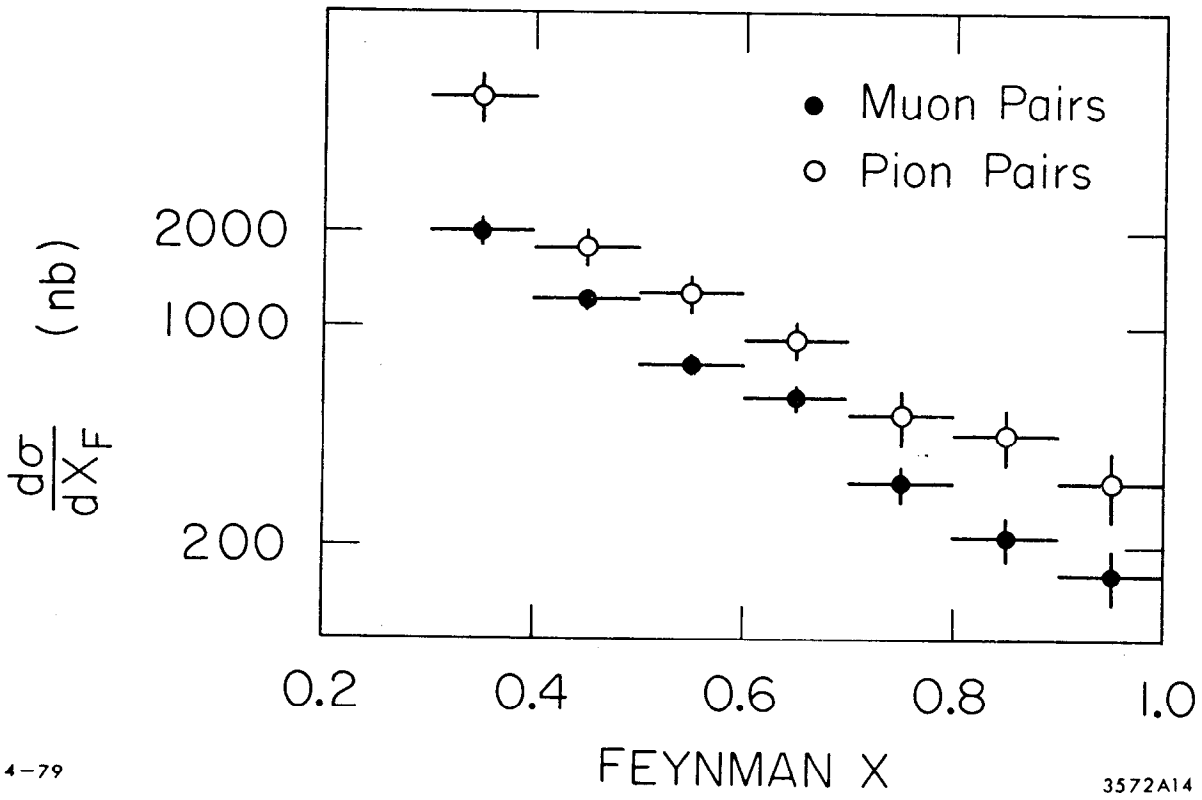
Muon Pairs
Pion Pairs
2000
1000
200
(nb)
dσ/dX_F
0.2
0.4
0.6
0.8
1.0
FEYNMAN X
4-79
3572A14

Fig. 11

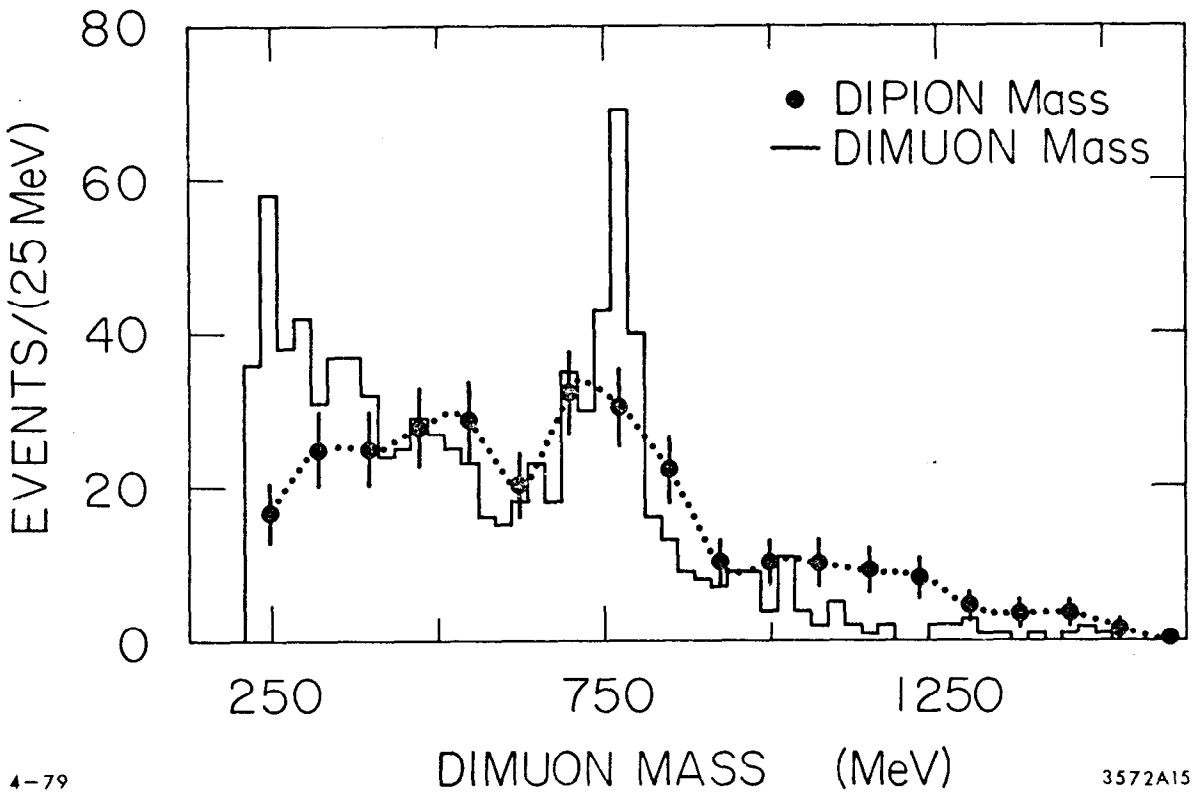
80
60
40
20
0
EVENTS/(25 MeV)
DIPION Mass
DIMUON Mass
250
750
1250
DIMUON MASS (MeV)
4-79
3572A15

Fig. 12

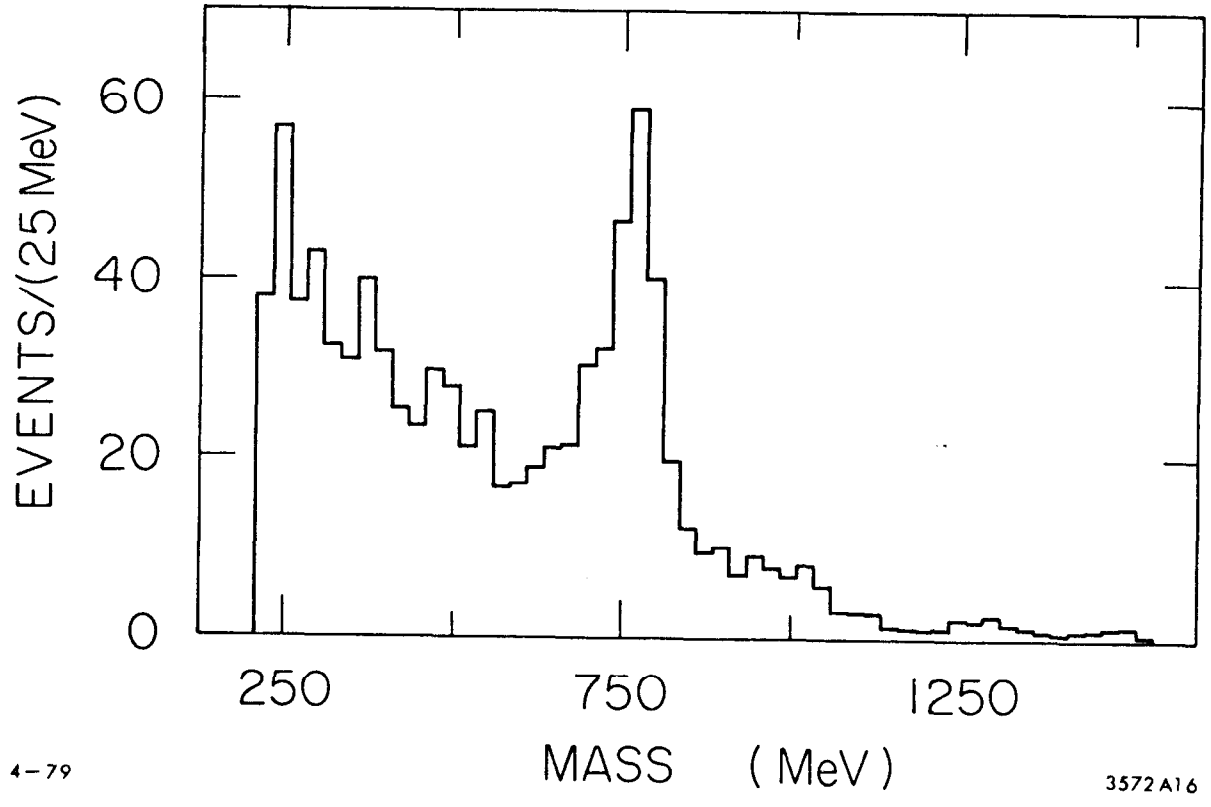

Fig. 13

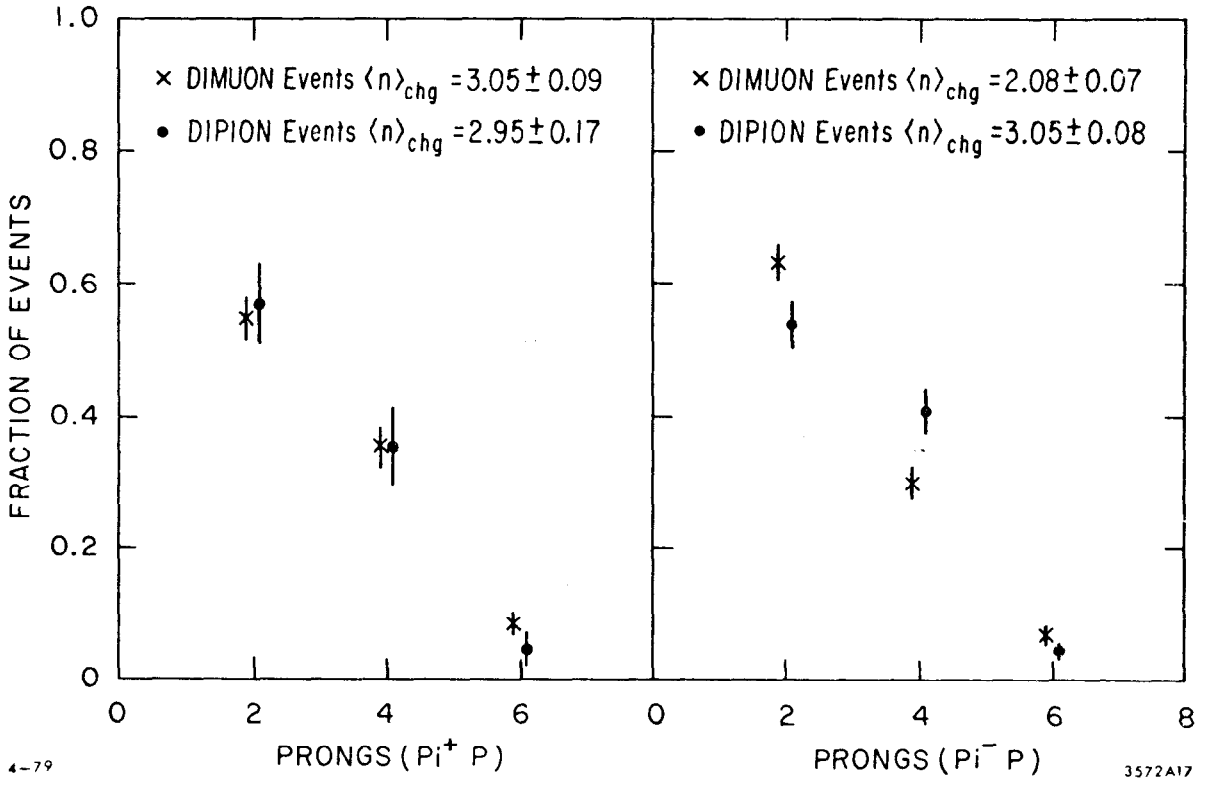
× DIMUON Events ⟨n⟩chg =3.05±0.09
• DIPION Events ⟨n⟩chg =2.95±0.17
× DIMUON Events ⟨n⟩chg =2.08±0.07
• DIPION Events ⟨n⟩chg =3.05±0.08
FRACTION OF EVENTS
1.0
0.8
0.6
0.4
0.2
0
0
2
4
6
0
2
4
6
8
PRONGS (Pi+ P)
PRONGS (Pi− P)
4-79
3572A17

Fig. 14

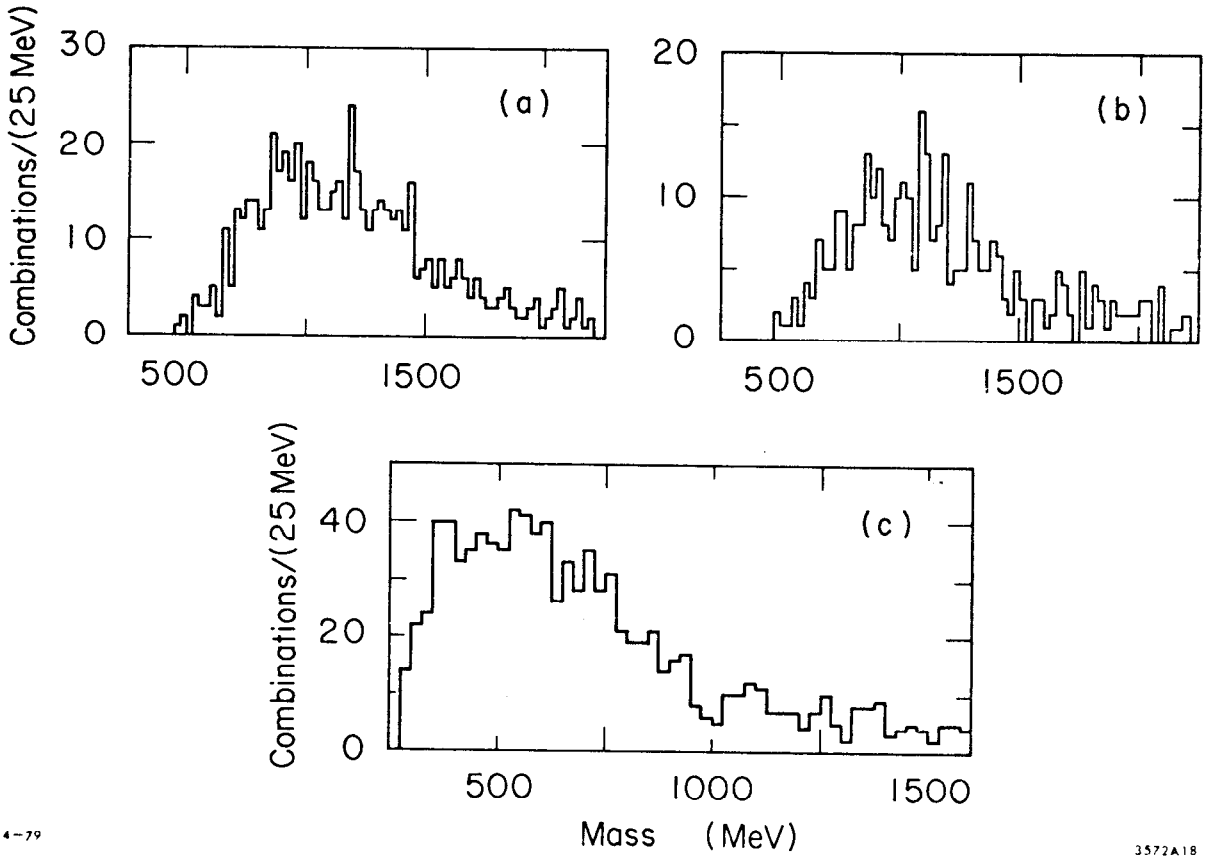
Combinations/(25 MeV)
30
20
10
0
500
1500
(a)
20
10
0
500
1500
(b)
Combinations/(25 MeV)
40
20
0
500
1000
1500
(c)
Mass (MeV)
4-79
3572A18

Fig. 15

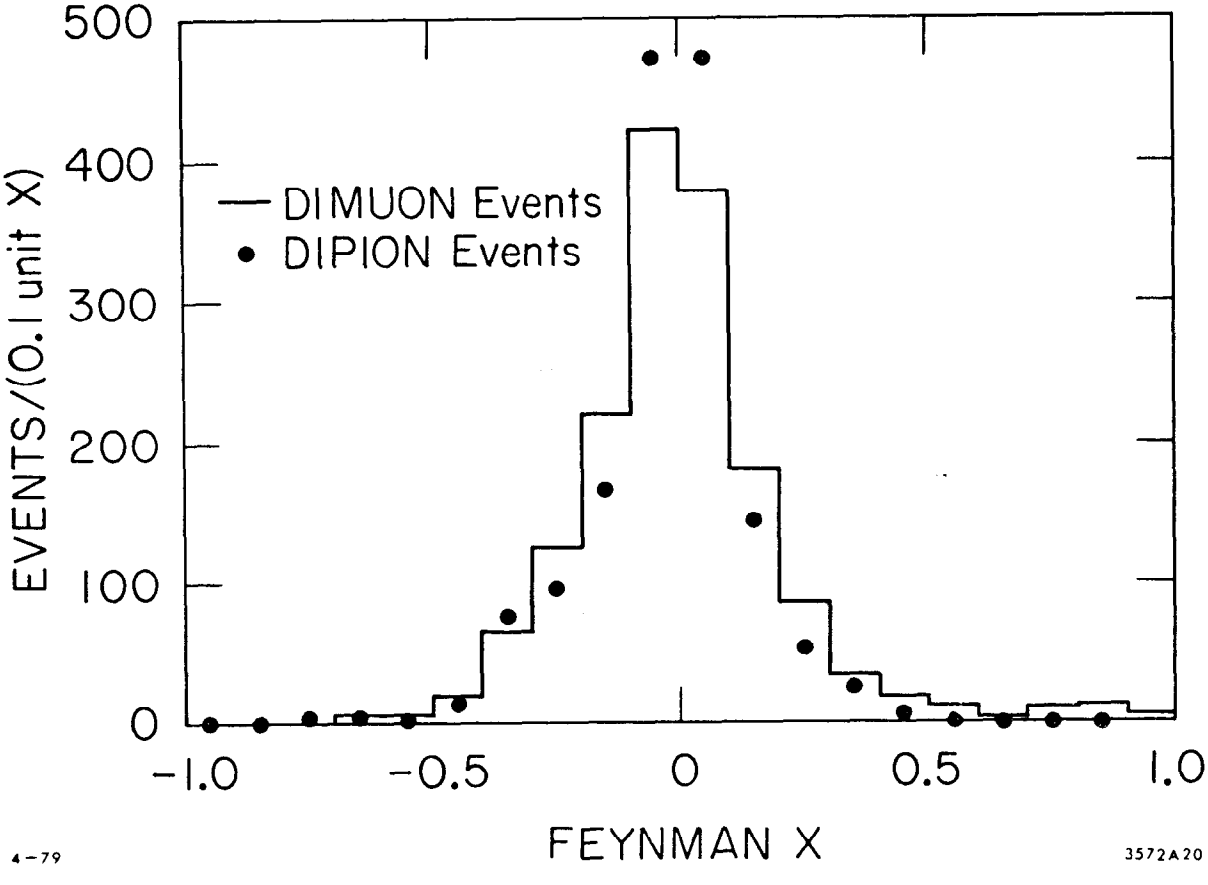
500
400
300
200
100
0
EVENTS/(0.1 unit X)
DIMUON Events
DIPION Events
-1.0
-0.5
0
0.5
1.0
FEYNMAN X
4-79
3572A20

Fig. 16

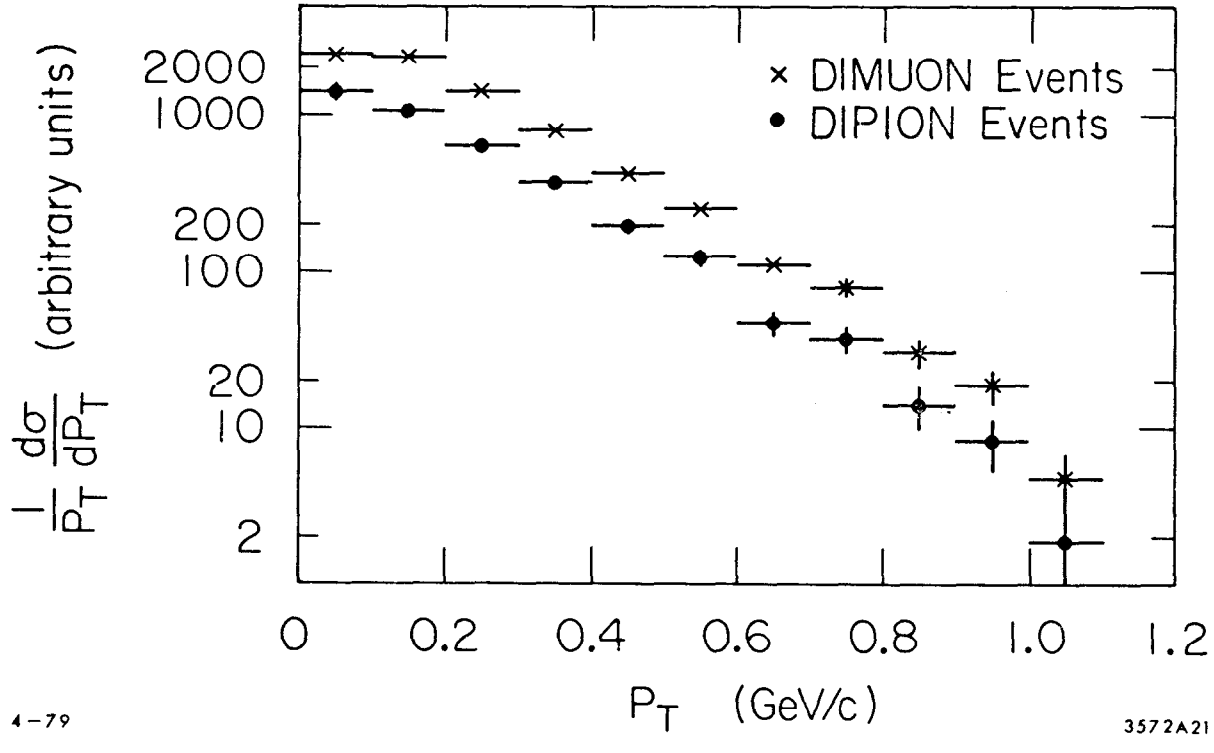
× DIMUON Events
• DIPION Events
2000
1000
200
100
20
10
2
0
0.2
0.4
0.6
0.8
1.0
1.2
$\frac{1}{P_T}\frac{d\sigma}{dP_T}$ (arbitrary units)
P_T (GeV/c)
4-79
3572A21

Fig. 17

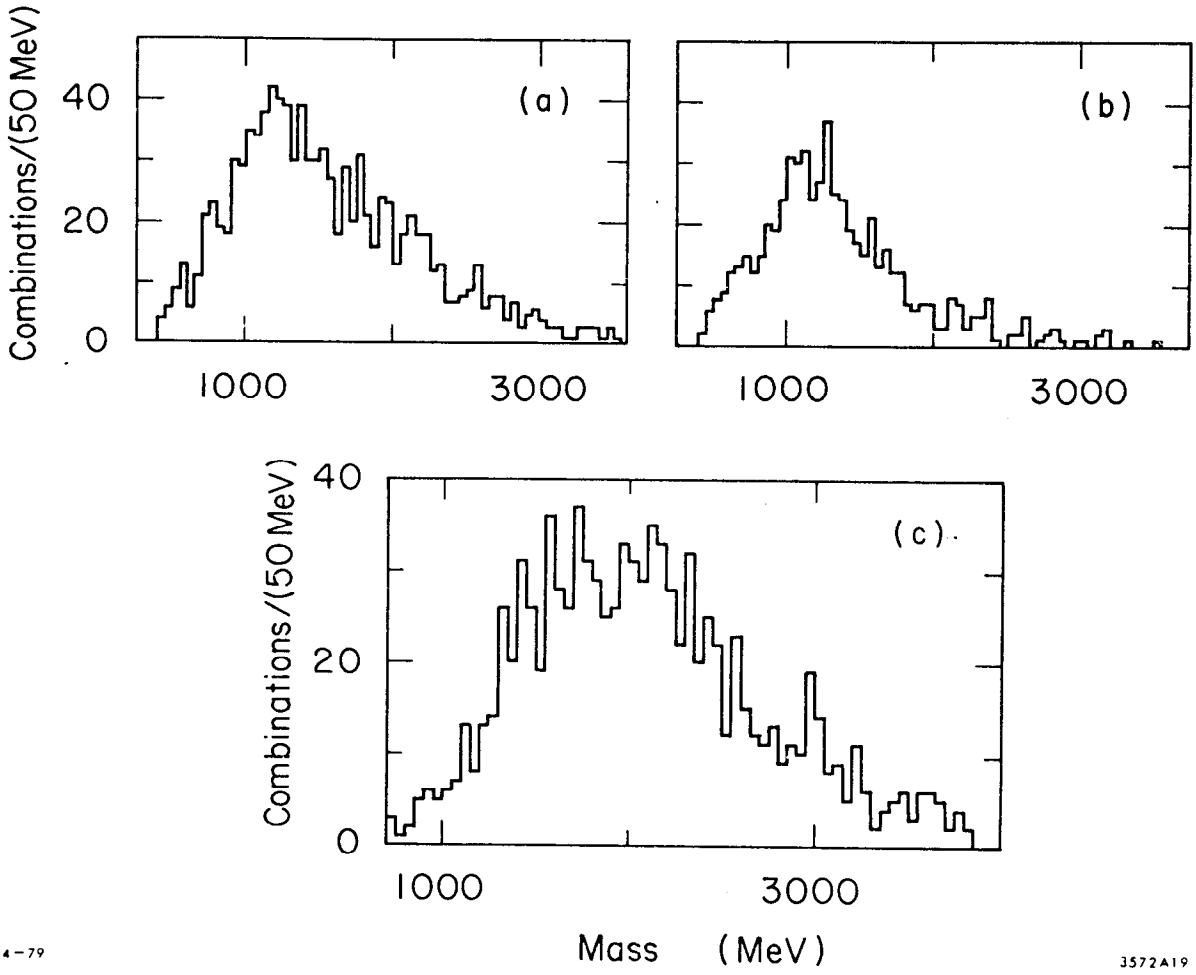
Combinations/(50 MeV)
40
20
0
(a)
1000
3000
(b)
1000
3000
Combinations/(50 MeV)
40
20
0
(c)
1000
3000
Mass (MeV)
4-79
3572A19

Fig. 18

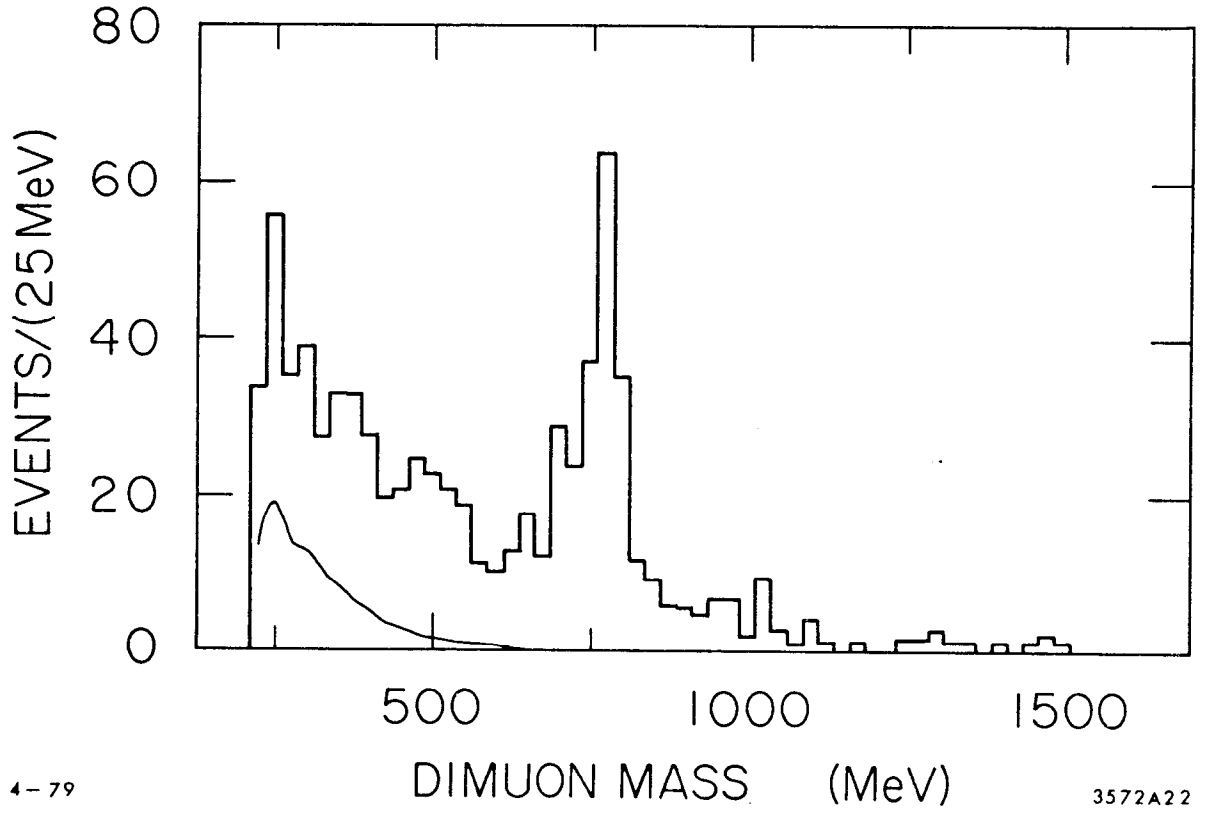
80
60
40
20
0
EVENTS/(25 MeV)
500
1000
1500
DIMUON MASS (MeV)
4-79
3572A22

Fig. 19

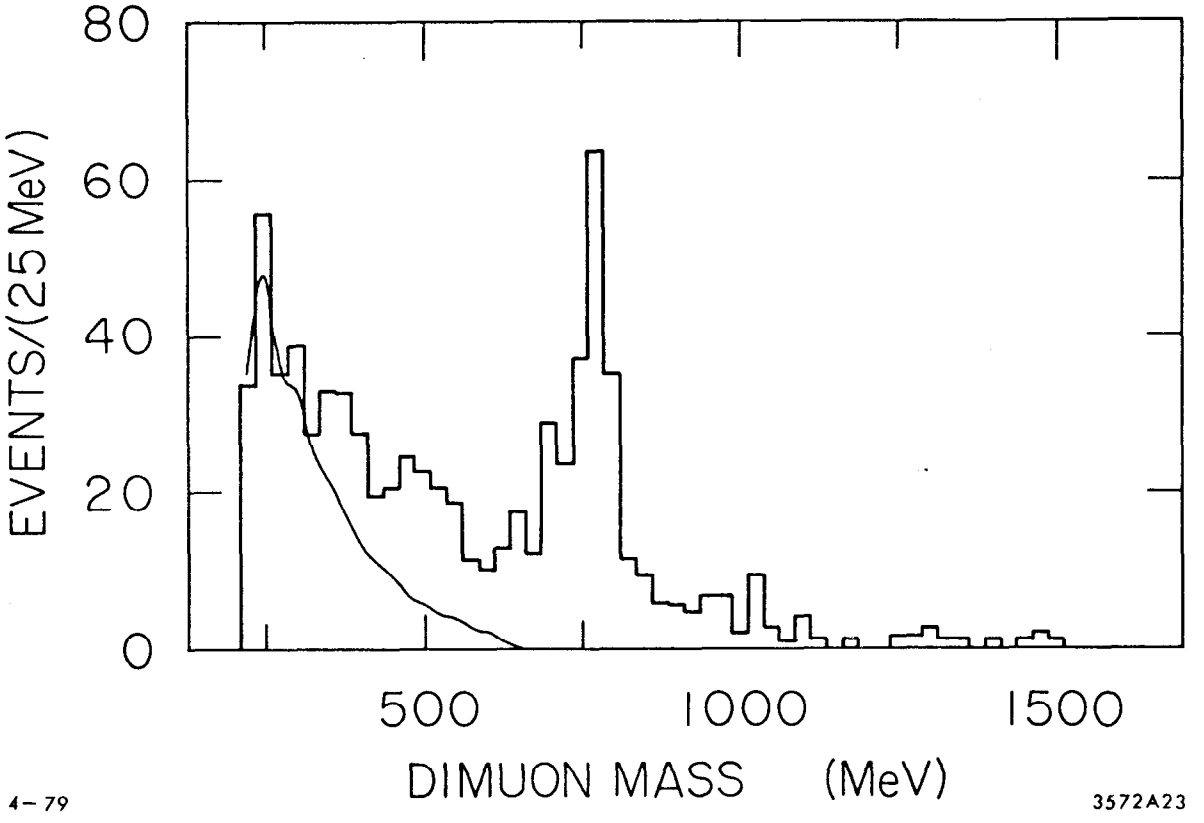
80
60
40
20
0
EVENTS/(25 MeV)
500
1000
1500
DIMUON MASS (MeV)
4-79
3572A23

Fig. 20

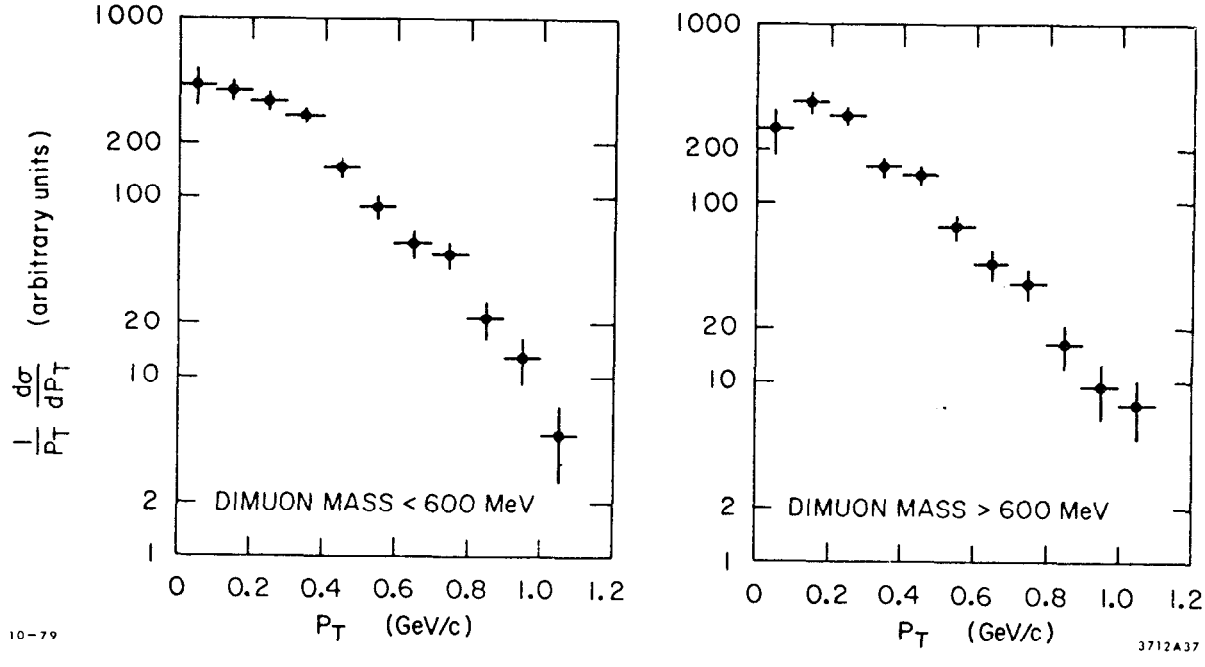
1000
200
100
20
10
2
1
$\frac{1}{P_T}\frac{d\sigma}{dP_T}$ (arbitrary units)
DIMUON MASS < 600 MeV
0
0.2
0.4
0.6
0.8
1.0
1.2
P_T (GeV/c)
DIMUON MASS > 600 MeV
P_T (GeV/c)
10-79
3712A37

Fig. 21

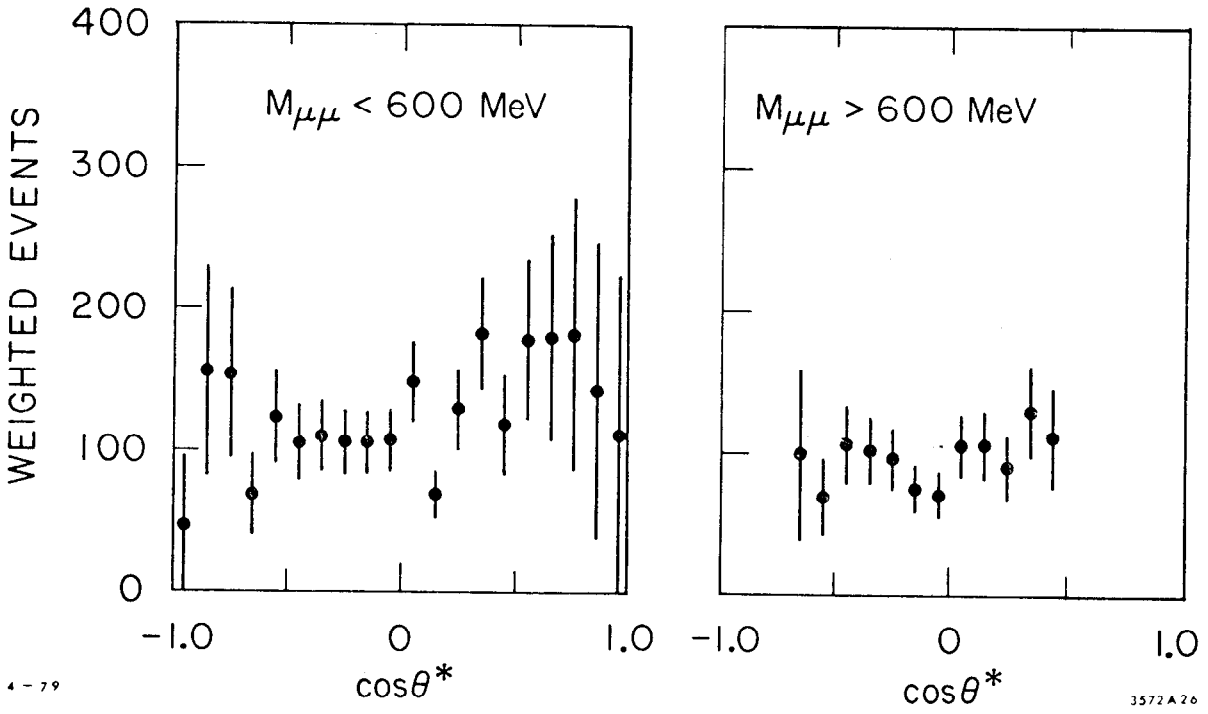
400
300
200
100
0
WEIGHTED EVENTS
$M_{\mu\mu}$ < 600 MeV
$M_{\mu\mu}$ > 600 MeV
-1.0
0
1.0
$\cos\theta^*$
4-79
3572A26

Fig. 22

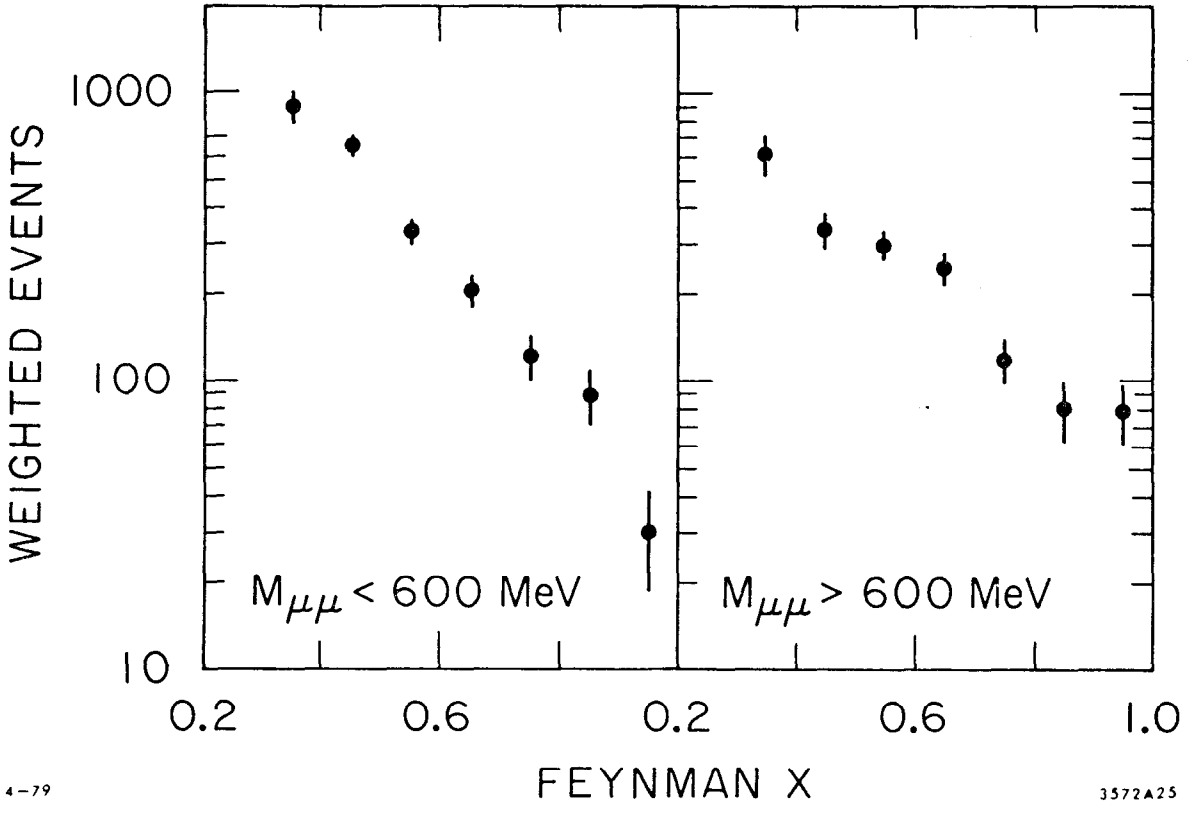
WEIGHTED EVENTS
1000
100
10
$M_{\mu\mu} < 600$ MeV
$M_{\mu\mu} > 600$ MeV
0.2
0.6
0.2
0.6
1.0
FEYNMAN X
4-79
3572A25

Fig. 23

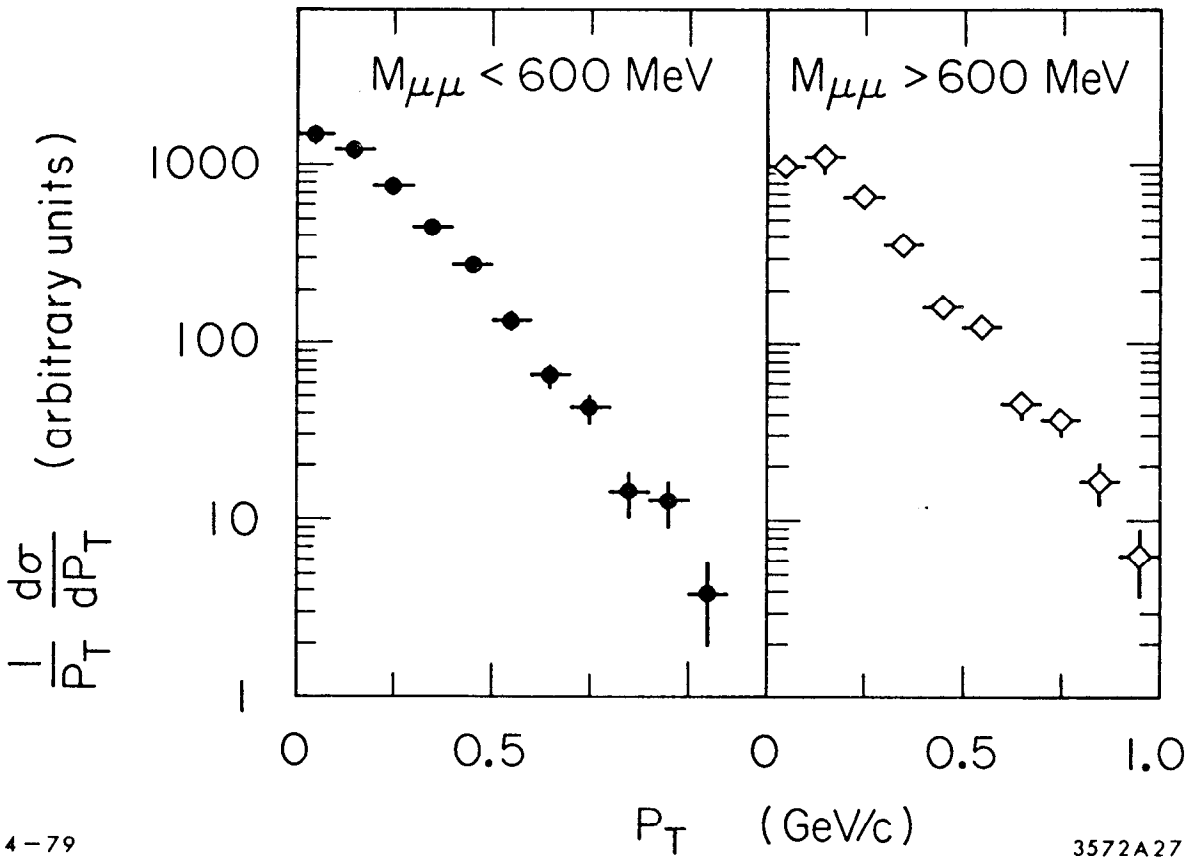
$M_{\mu\mu} < 600$ MeV
$M_{\mu\mu} > 600$ MeV
1000
100
10
1
$\frac{1}{P_T}\frac{d\sigma}{dP_T}$ (arbitrary units)
0
0.5
0
0.5
1.0
P_T (GeV/c)
4-79
3572A27

Fig. 24

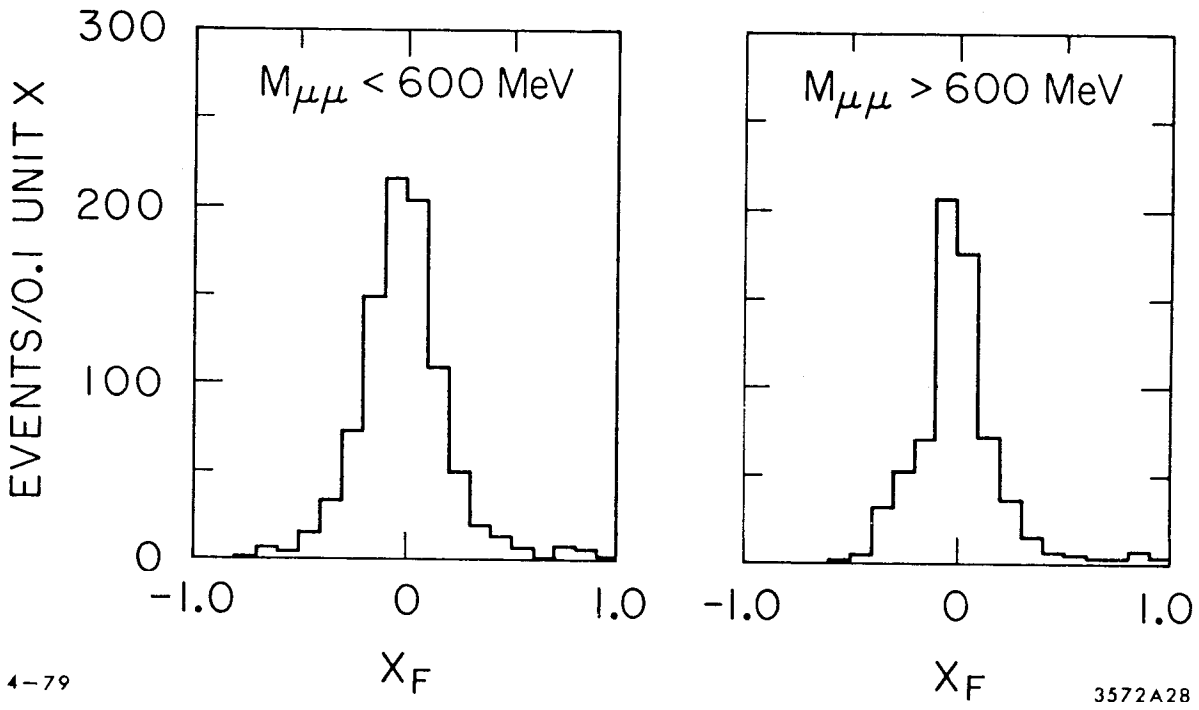
300
200
100
0
EVENTS/0.1 UNIT X
$M_{\mu\mu}$ < 600 MeV
$M_{\mu\mu}$ > 600 MeV
-1.0
0
1.0
X_F
4-79
3572A28

Fig. 25

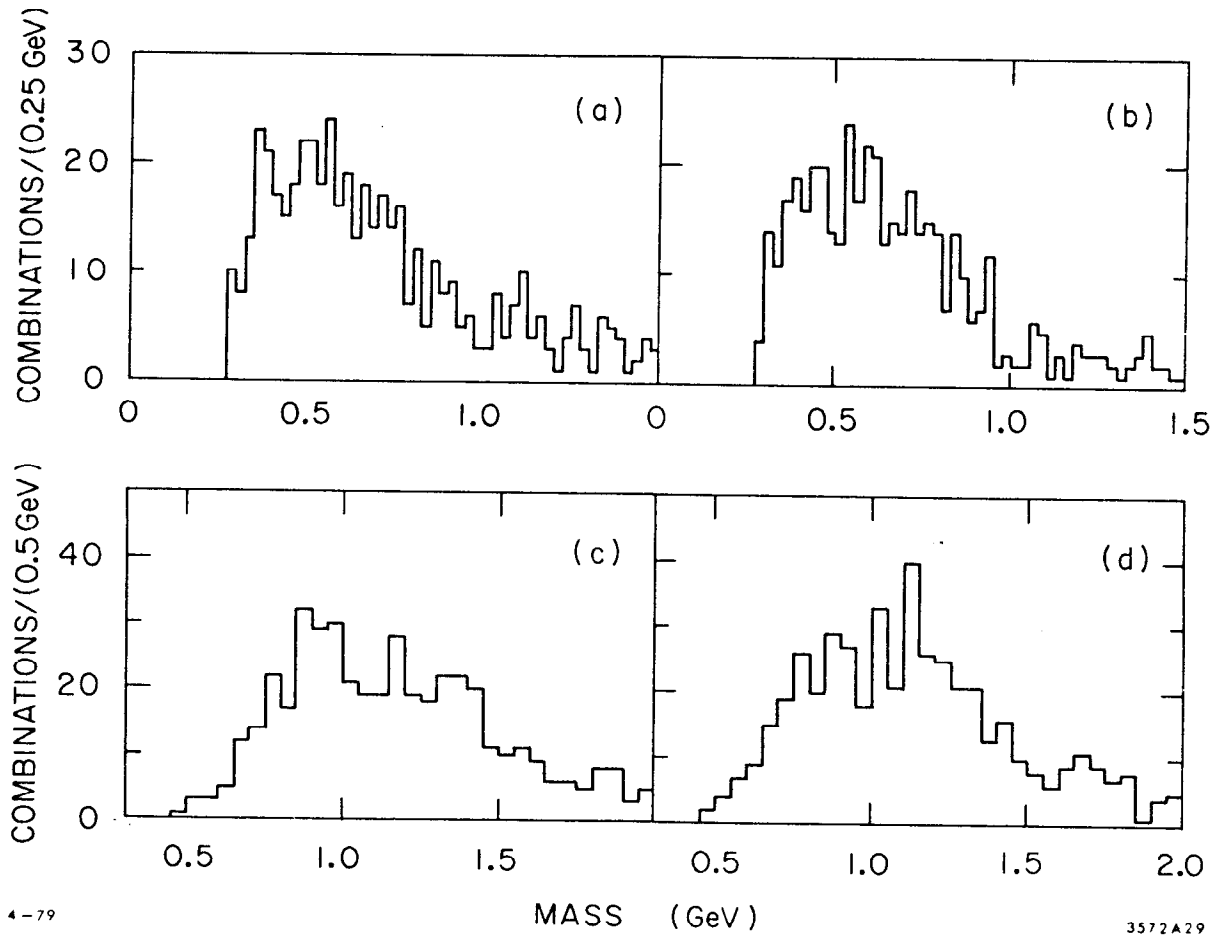
COMBINATIONS/(0.25 GeV)
30
20
10
0
(a)
(b)
0
0.5
1.0
0
0.5
1.0
1.5
COMBINATIONS/(0.5 GeV)
40
20
0
(c)
(d)
0.5
1.0
1.5
0.5
1.0
1.5
2.0
MASS (GeV)
4-79
3572A29

Fig. 26

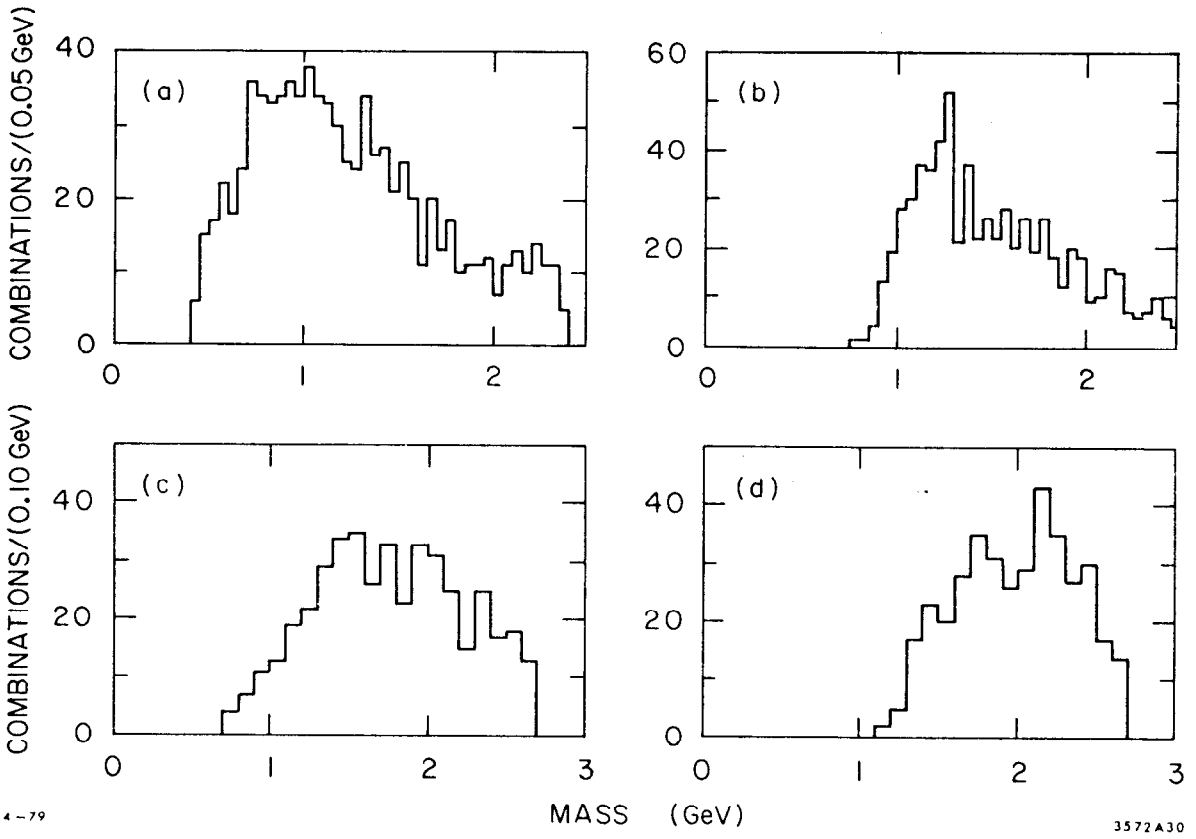
COMBINATIONS/(0.05 GeV)
COMBINATIONS/(0.10 GeV)
(a)
(b)
(c)
(d)
MASS (GeV)
4-79
3572A30

Fig. 27

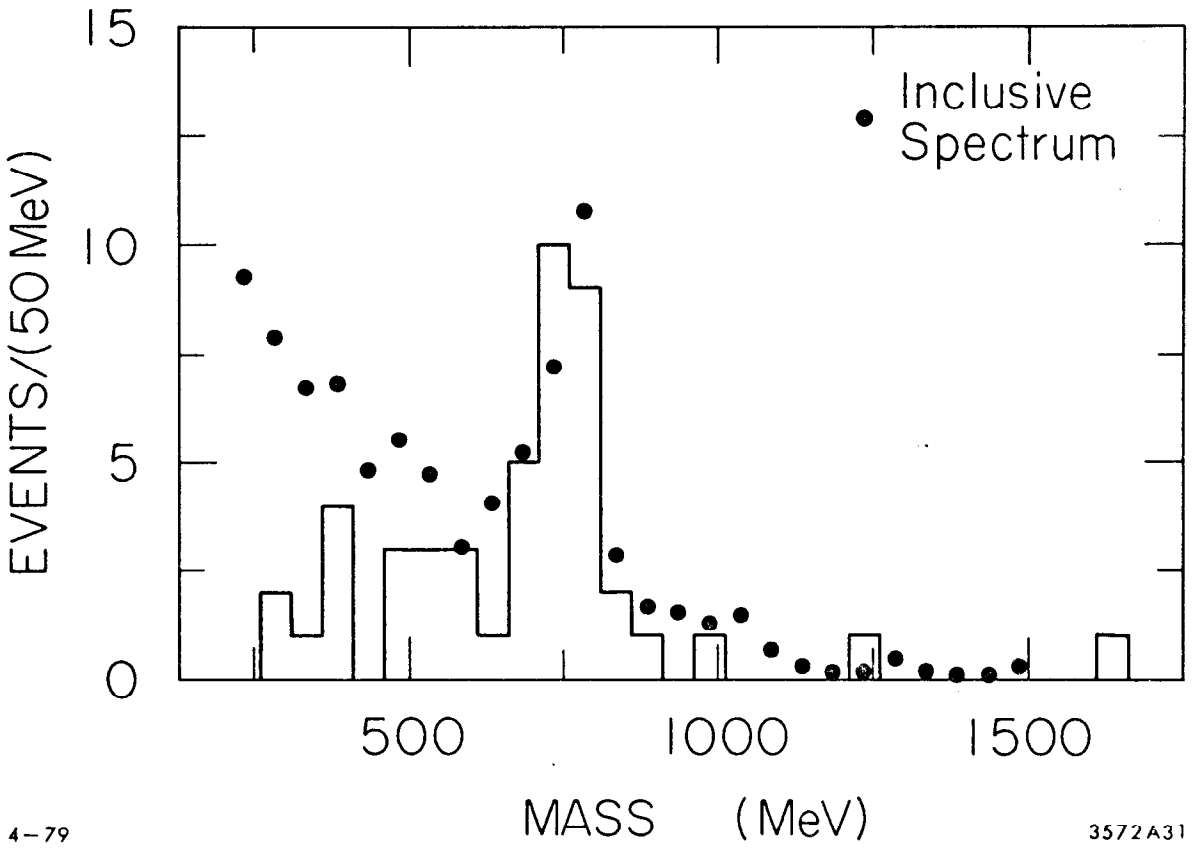
15
10
5
0
EVENTS/(50 MeV)
Inclusive
Spectrum
500
1000
1500
MASS (MeV)
4-79
3572A31

Fig. 28

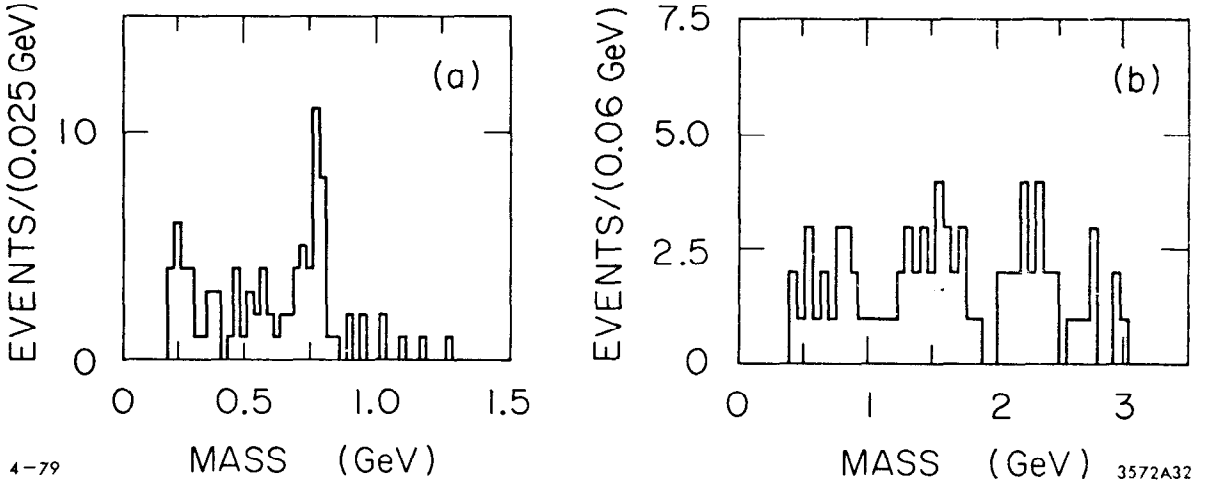
EVENTS/(0.025 GeV)
10
0
(a)
0
0.5
1.0
1.5
MASS (GeV)
4-79
EVENTS/(0.06 GeV)
7.5
5.0
2.5
0
(b)
0
1
2
3
MASS (GeV)
3572A32

Fig. 29

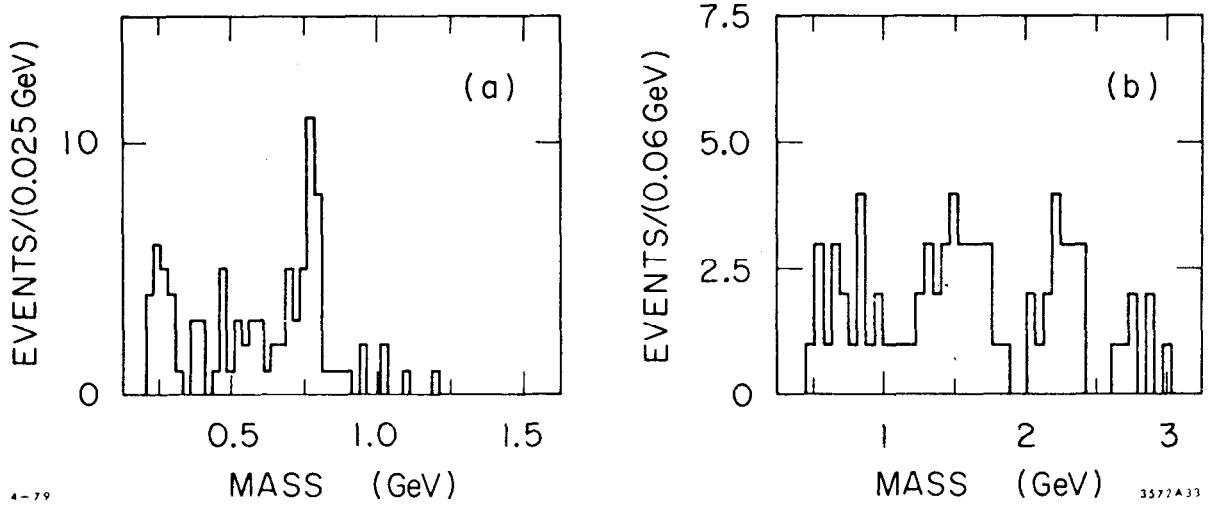
EVENTS/(0.025 GeV)
10
0
(a)
0.5
1.0
1.5
MASS (GeV)
4-79
EVENTS/(0.06 GeV)
7.5
5.0
2.5
0
(b)
1
2
3
MASS (GeV)
3572A33

Fig. 30

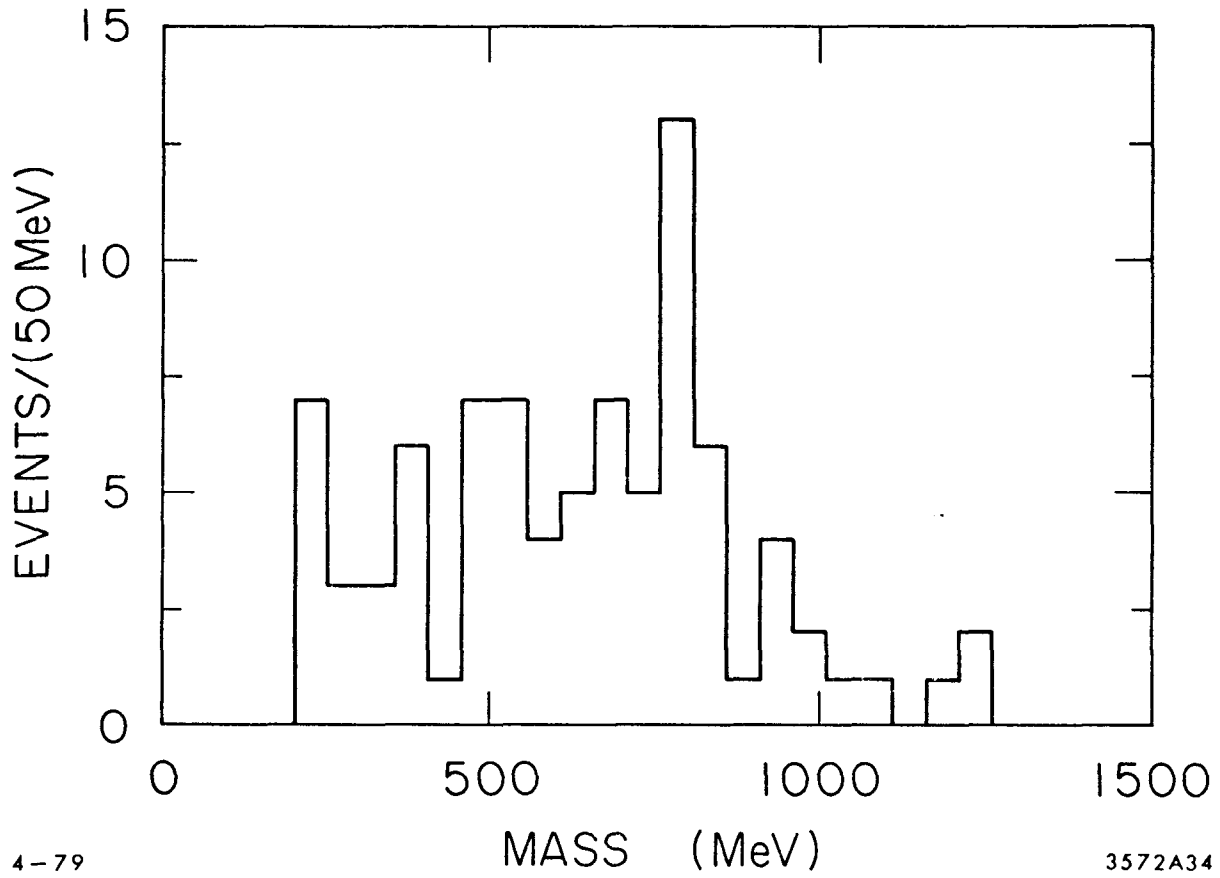

Fig. 31

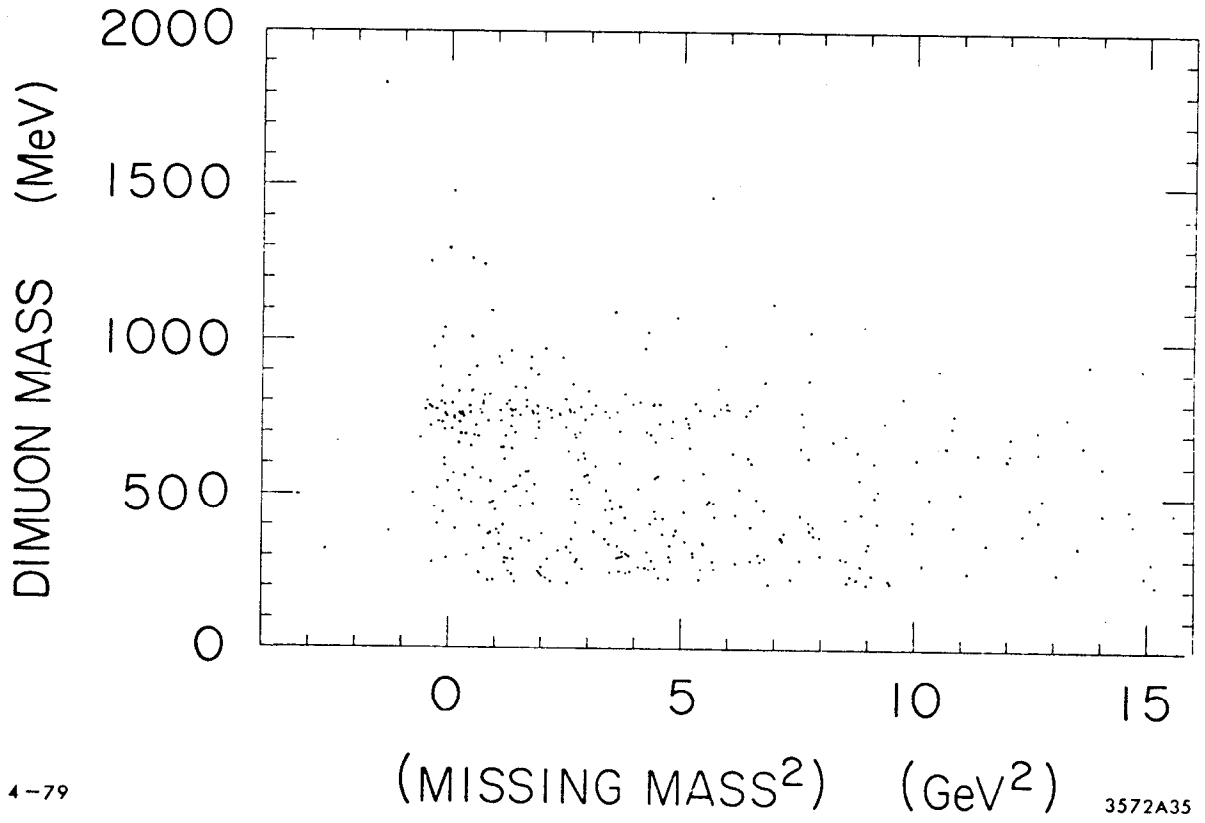
2000
1500
1000
500
0
DIMUON MASS (MeV)
0
5
10
15
(MISSING MASS^2) (GeV^2)
4-79
3572A35

Fig. 32

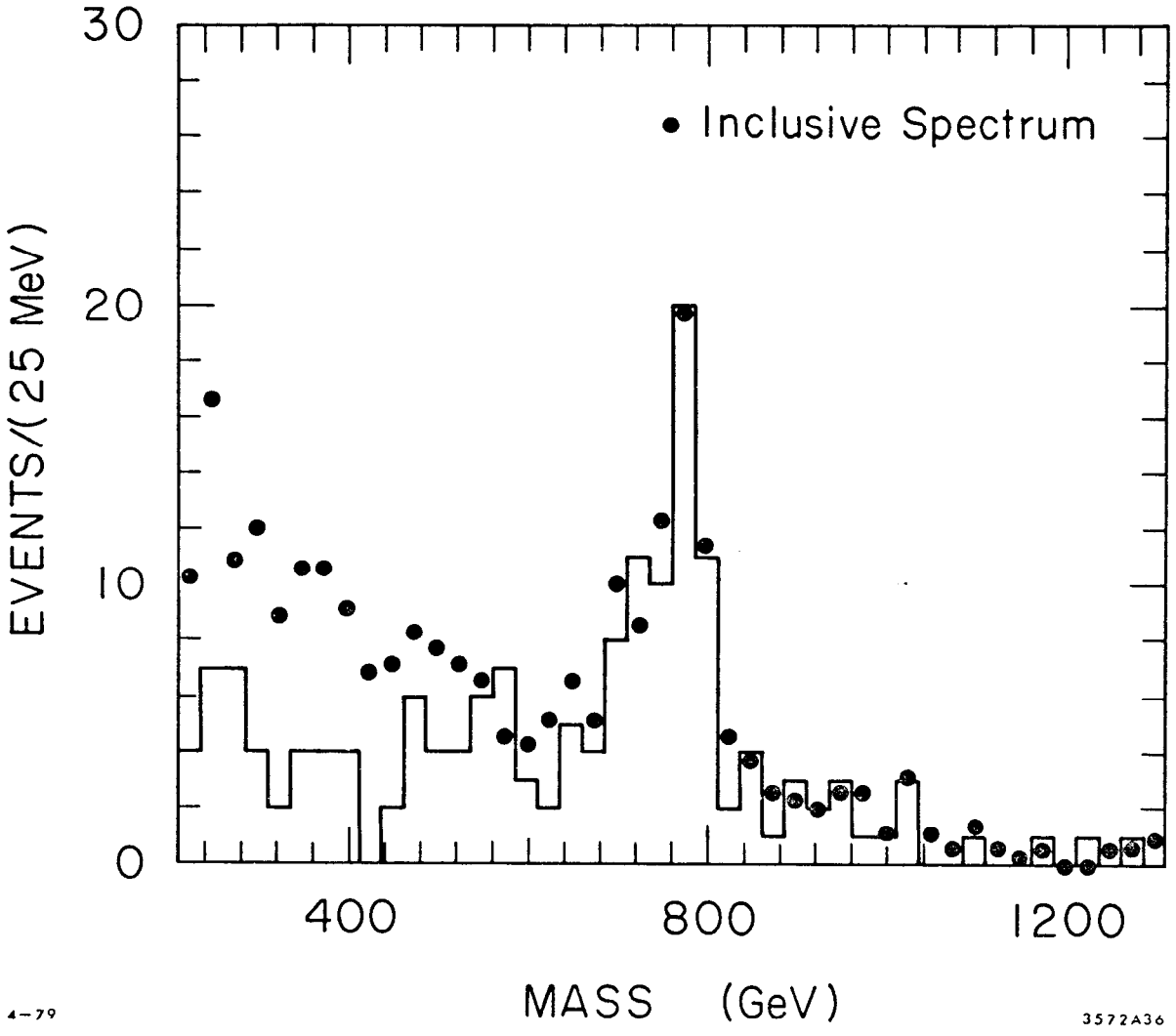
30
20
10
0
EVENTS/(25 MeV)
• Inclusive Spectrum
400
800
1200
MASS (GeV)
4-79
3572A36

Fig. 33

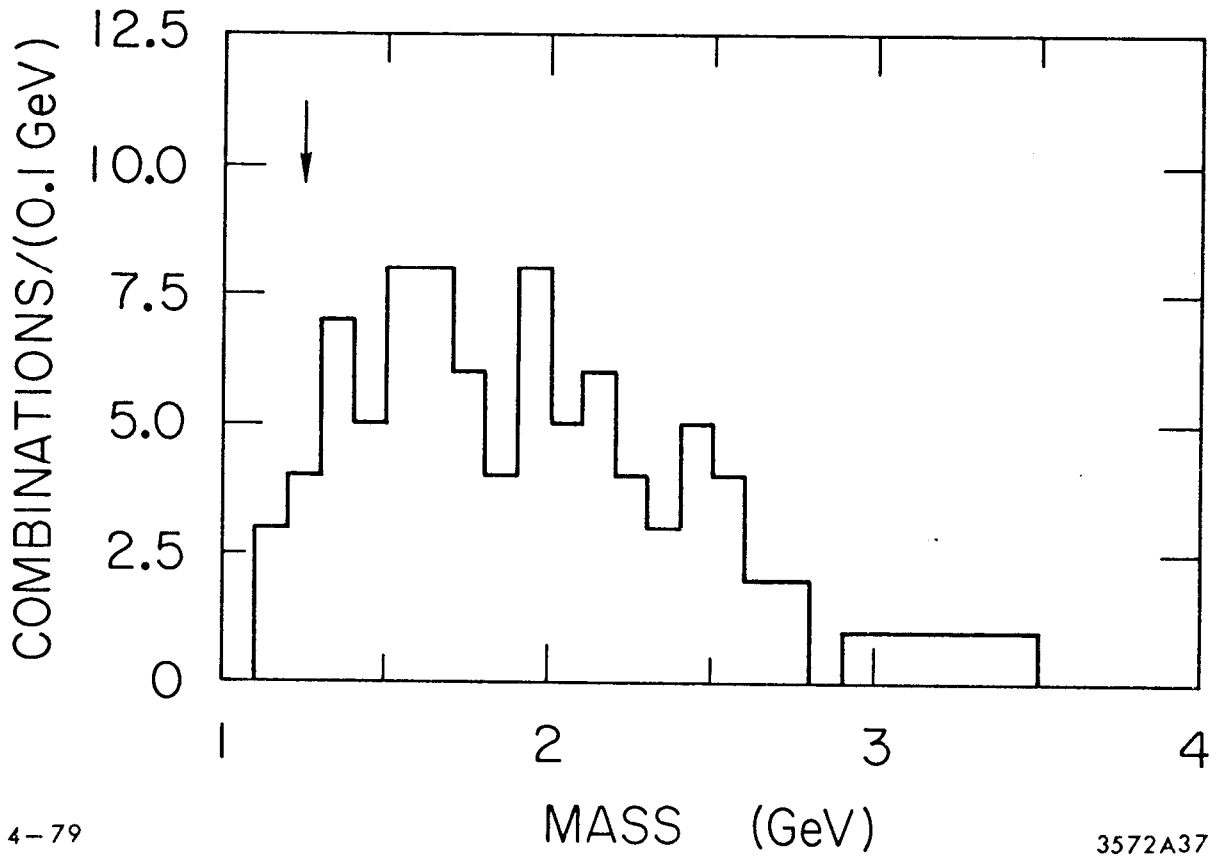
12.5
10.0
7.5
5.0
2.5
0
COMBINATIONS/(0.1 GeV)
1
2
3
4
MASS (GeV)
4-79
3572A37

Fig. 34

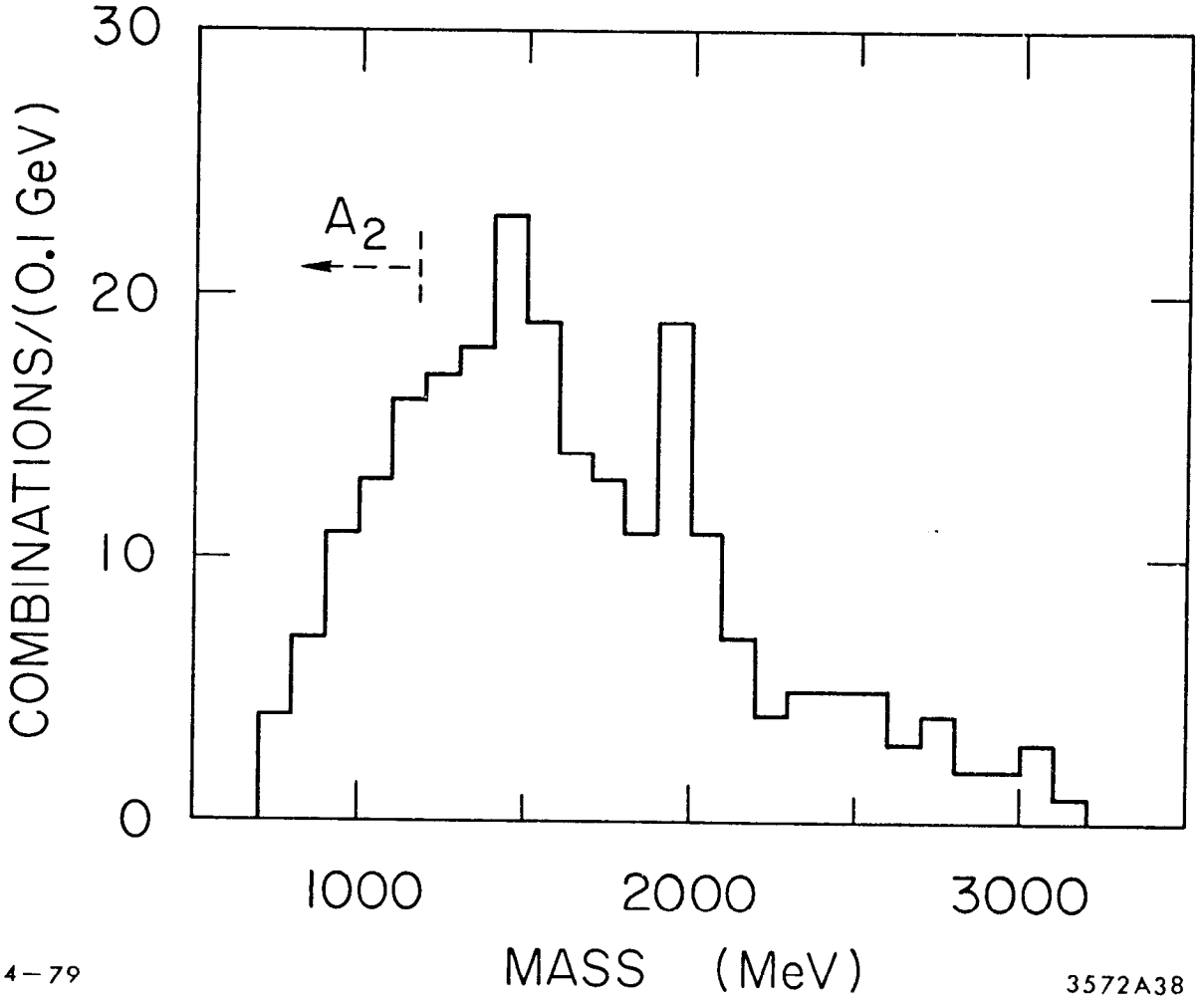
30
20
10
0
COMBINATIONS/(0.1 GeV)
A_2
1000
2000
3000
MASS (MeV)
4-79
3572A38

Fig. 35

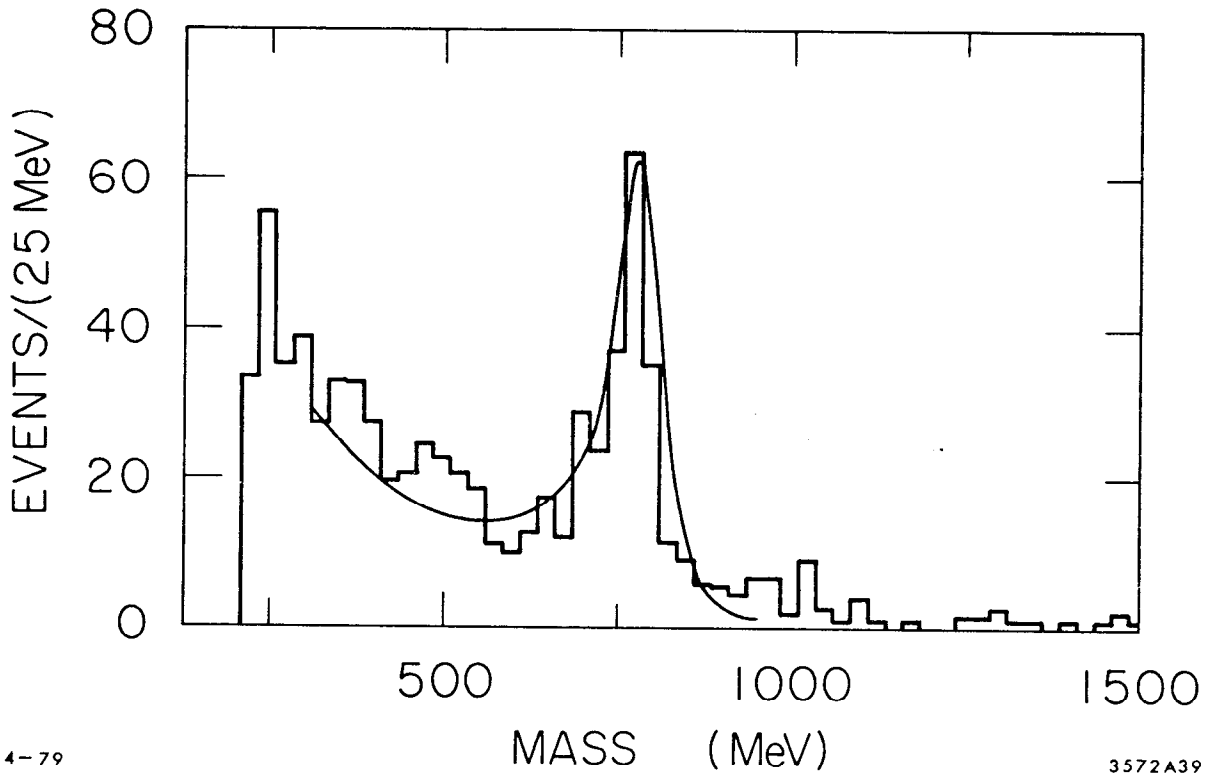

Fig. 36

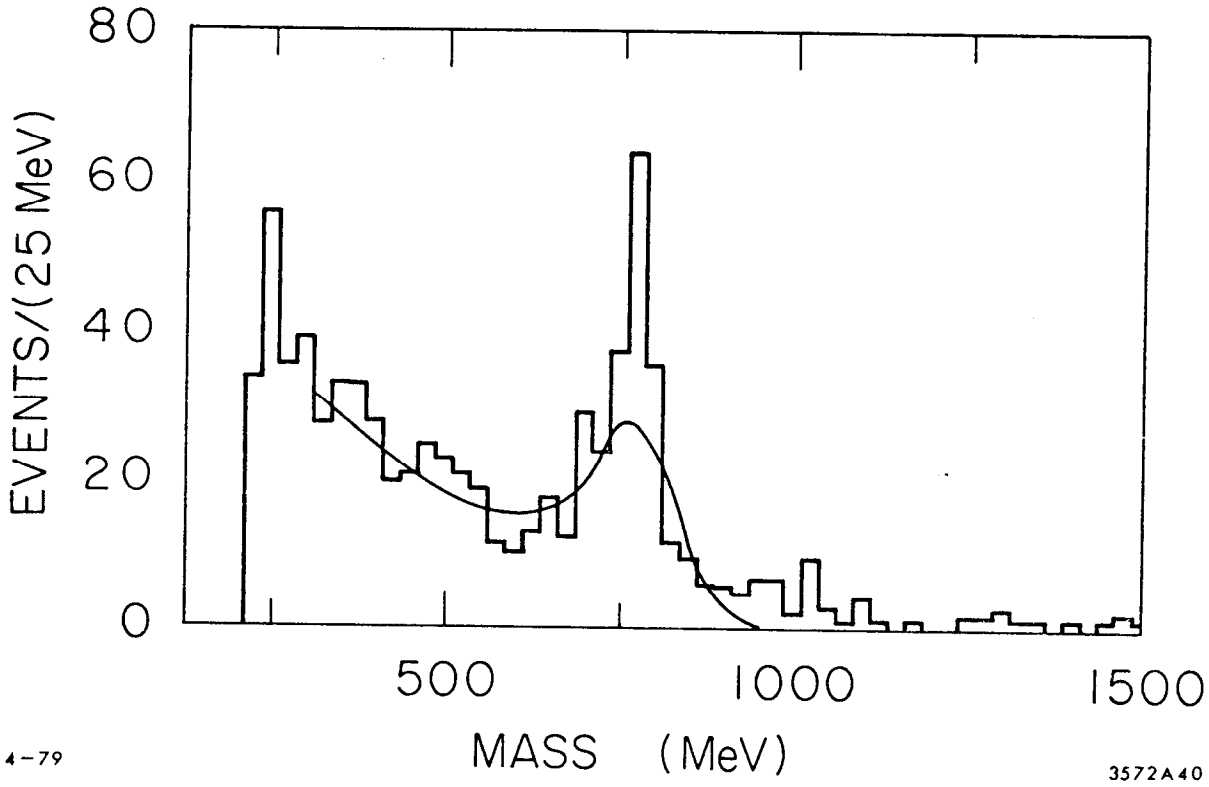

Fig. 37